DEVELOPMENT OF TRANSPARENT COMPOSITE LAMINATES AND EYALUATION OF MODE-I STRESS INTENSITY FACTOR USING PHOTO - ORTHOTROPIC ELASTICITY

by

NACHIKETA TIWARI

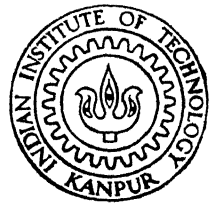

DEPARTMENT OF MECHANICAL ENGINEERING

INDIAN INSTITUTE OF TECHNOLOGY KANPUR

DECEMBER, 1990

DEVELOPMENT OF TRANSPARENT COMPOSITE LAMINATES AND EYALUATION OF MODE-I STRESS INTENSITY FACTOR USING PHOTO - ORTHOTROPIC ELASTICITY

A Thesis Submitted

in Partial Fulfilment of the Requirements
for the Degree of

MASTER OF TECHNOLOGY

by

NACHIKETA TIWARI

to the

DEPARTMENT OF MECHANICAL ENGINEERING

INDIAN INSTITUTE OF TECHNOLOGY KANPUR

DECEMBER, 1990

CERTIFICATE

This is to certify that this thesis entitled "**Development of Transparent Composite Laminates and Evaluation of Mode-I Stress Intensity Factor Using Photo-Orthotropic Elasticity**", by Nachiketa Tiwari is a record of the work carried out under my supervision and has not been submitted elsewhere for a degree.

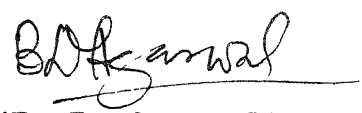

(B. D. Agarwal)

Professor

Department of Mechanical Engineering

Indian Institute of Technology

Kanpur-208 016

December, 1990.

ACKNOWLEDGMENTS

I am extremely grateful to **Prof. B. D. Agarwal**, for his extremely valuable guidance and constructive criticism throughout the present investigations. He has been a constant source of inspiration and generosity to me, for which I shall be ever indebted to him.

I am also extremely thankful to **Dr. K. Ramesh** who was ever willing to help me on all the fronts. His guidance and help, especially on issues related to photoelasticity, were invaluable.

I express my sincere thanks to **Dr. N. N. Kishore**, Co-ordinator of the Experimental Stress Analysis Laboratory, for extending the facilities of the lab to me. Thanks are also due to **Prof. Prashant Kumar**, for his useful discussions and encouragement during the investigations.

I am also thankful to **Mr. Diwakar**, of the ESA Lab. for his valuable assistance in carrying out the experimental work. I am also indebted to the co-operation provided by Messrs. **K. K. Bajpai, S. L Srivastava, D. N. Sarkar, R. C. Maurya and Sudhir Srivastava** of the ESA Lab.

I appreciate the help provided by the **Advanced Center for Material Sciences** and the **Physics Department** by extending their laboratory facilities, needed for characterizing the newly developed composite material. Lastly, I thank all my well wishers who have helped me directly or otherwise in the present work.

Nachiketa Tiwari

CONTENTS

LIST OF FIGURES

ABSTRACT

Fibrous composites are fast replacing conventional engineering materials in various industries. Understanding the mechanism of fracture for these orthotropic materials is a problem. The theory of orthotropic photoelasticity can be employed for an efficient analysis of fracture phenomena in such materials. However, usage of this tool of experimental mechanics is possible only if a suitable model material is available.

It is in this context that a model material exhibiting orthotropic properties, for photoelastic studies has been developed. Its optical properties have been found to be much better than those of the materials developed earlier.

Further, the principles of orthtropic fracture mechanics have been employed to determine the value of stress intensity factor for unidirectional laminates. Knowledge of this parameter is very important, since it can be used as a tool to understand the mechanism of fracture in composites. The values of S.I.F for the unidirectional laminate were found to be reasonably correct.

It is expected that the newly developed model material and principles of orthotropic photoelasticity will meet the growing demand for an efficient stress and fracture analysis of fibrous composites.

1 INTRODUCTION

1.1 Importance of Composite Materials:

The word "**composite**" means 'consisting of two or more distinct parts' [1]. Thus a material having two or more distinct constituent materials may be considered a composite material. It is only when the constituent phases have significantly different physical properties and thus the composite properties are noticeably different from the constituent properties that we have come to recognize these materials as composites.

Composite materials have slowly emerged as easily workable engineering materials and are now quite commonly available and used, globally. Modern engineering industry finds application of these materials in areas as different as low technology applications like panels for doors to high-tech applications viz. space programs and aircraft industry.

The success of fiber composites results from the ability to make use of the outstanding strength, stiffness, and low specific gravity of fibers such as glass, graphite, or Kevlar. When outstanding mechanical properties are combined with the unique flexibility in design capability and ease of fabrication that composites offer, it is no wonder that their growth rate has far surpassed other materials. Another unique characteristic that distinguishes composites from other materials is that in the case of fiber composites, at the same time the structure or component is manufactured, the material itself is being synthesized.

1.2 Stress Analysis for Composite Materials:

A material as important as composite needs to be used with care. This need becomes all the more crucial, since the single most important reason for their usage is their lightness. Hence, any design which is oversafe, will increase the weight of the system disadvantageously. For better utilization of the material, it is important that the stress field in the system is optimized. Hence the need for detailed stress analysis.

There are several methods to find stresses in a composite laminate. Some of them are; photo-elasticity, strain-gage techniques, holography, moire's method, FEM.

1.3 Photoelasticity and Composites:

Photoelasticity, a well established branch of experimental mechanics, has been successfully tried for the analysis of isotropic materials.

The advantage of photoelasticity is that it is a whole-field technique. Consequently, one single experiment in photoelasticity gives a wealth of data. Hence the reliability of each experiment in photoelasticity is definitely much more than an experiment based on single-point techniques.

However, isotropic transmission photoelasticity runs into trouble when composite materials are the field of study. It is so since composite materials are anisotropic in nature. Consequently, the laws of conventional transmission photoelasticity fail to predict the mechanical behaviour of composite materials.

In light of these facts, it becomes very essential to modify the laws of isotropic photoelasticity. In this field, several investigators have made their significant contributions. Consequently, a newer version of photo-elasticity, "**orthotropic photoelasticity**" has emerged.

Investigations in the field of orthotropic photoelasticity can be categorized into three broad areas.

1. Development of suitable composite model material for photoelastic investigations.
2. Development of suitable stress-optic laws and strain-optic laws which are accurate as well as easy to handle.
3. Using the developments mentioned in 1 and 2 to analyze physically realizable problems.

1.4 Fracture in Composites:

The importance of fracture mechanics, especially linear-elastic-fracture-mechanics is well documented. This has been dealt in great detail by Liebowitz [9], Broek [1Ø], Kobayashi [11] and Rolfe [12]. Although most of the work done in this area has been done for isotropic materials, the significance of anisotropic materials like composites in the modern industry, has impelled several investigators to establish the theory of anisotropic fracture mechanics, and furthermore, to investigate their fracture mechanisms.

In these studies the model material is assumed to be homogeneous and orthotropic if either the structure is free from flaws which may be the cause of an eventual failure initiation, or the structure may have a flaw whose size is large in

comparison with the local micro-structural parameters such as fiber diameter and the distance between two adjacent fibers. Otherwise, in failure initiation studies the material has to be treated as a non-homogeneous continuum containing local flaws with certain geometries.

A distinguishing feature of composites, from the view of structural failure, is that these materials are generally not isotropic with respect to their fracture resistance. Furthermore, in a majority of cases, the planes of orthotropy are generally also the planes of weak fracture resistance. Thus in orthotropic materials regardless of the overall geometry and the loading conditions, the fracture propagation would be either along a plane of orthotropy or would have zig-zag path. This is in sharp contrast to isotropic materials, where the plane of fracture quite often coincides with the plane(s) of maximum principal stresses. This is one very important reason for carrying out an in-depth study of the fracture-phenomena of composites.

A very important parameter in fracture studies is the **stress-intensity factor**. Knowledge of this factor aids in predicting the stress-field near the crack-tip in the material under observation. However, usage of this parameter is justified as long as the zone of plasticity in the vicinity of the crack tip is small enough. For ductile metals, the zone of plasticity is very large. However, plastic yielding in the case of composite materials is almost negligible. Thus, the relevance of stress-intensity factor for the understanding of fracture in composites is all the more important.

1.5 Present Work and Its Scope:

The significance of **stress-intensity factor** for composites has been discussed in the preceding section. So far the method of photo-elasticity, despite its advantages as discussed above, has not been employed with much of success for the determination of this important parameter.

One very important reason for this is that the availability of a suitable orthotropic material with a high degree of transparency is very difficult. As a part of the present investigation, a suitable photoelastic model material for orthotropic materials has been developed. The method though tedious, gives very good results. The details of this development are given in the second chapter of this thesis.

In view of the tedious process of the fabrication of the model material, optimum usage of this material, especially during its characterization, is very important. The relevant details of the characterization of the model material have been discussed in the third chapter.

In the fourth chapter, stress intensity factor for unidirectional laminates has been evaluated, using orthotropic photoelasticity. The method followed for this purpose has been found to be quite reliable. However, the process is time consuming. The fifth and the final chapter suggests various ways of automating this process and making it even more rigorous.

2 DEVELOPMENT OF TRANSPARENT COMPOSITES :

2.1 Introduction :

The first step in applying transmission photoelasticity method to the stress analysis of orthotropic material involves the development of a suitable model material. The properties desirable of a model material for photo-orthotropic-elasticity applications are :

1. The model material should be transparent and homogenous.
2. Volume fraction of fibers should be high enough to ensure **sufficient orthotropy** in the model. However, fiber volume fraction should not be too high so as to reduce its sensitivity.
3. The model material should be designed to exhibit adequate amount of birefringence. Use of a very thin model will result in inadequate response of the stressed model to polarized light. On the other hand, use of a very thick model causes appreciable variation of the stress-field in the thickness direction. This is significant during oblique incidence.

The first two requirements were met by controlling the fabrication process and varying the constituents of the model while the third requirement was met by controlling its thickness.

2.2 Review of The Past Development Transparent Composites:

First attempt to prepare transparent orthotropic material was made by **Horridge** [9]. He matched the refractive indices of glass and polyester resin approximately to achieve the desired

results. Vinyl di-chlorosilane was used to improve the glass-resin bonding. **Pih and Knight** [2] used E-glass fibers for this purpose. They used **wet filament winding process**. The entire process was carried out in vacuum to ensure removal of air bubbles. **Sampson** [3] also made attempts in similar directions. However, he used **dry filament winding process.**

Dally and Prabhakaran [4] prepared large sheets of transparent composites by using E-glass fibers and Paraplex P-444H resin. Thirty percent styrene was added to resin to ensure a close match between the refractive indices of glass and resin. Dally et. al. characterized these sheets as **sufficiently transparent. FMC Corporation** [5] has developed transparent composites by using two different special formulations. Usage of silane coupling agents is advised in these formulations to ensure that laminates "retain there clarity upon aging [5]". **Pipes and Rose** [6] applied tension in the fibers to ensure proper alignment of fibers. However, the model material developed by them was not homogenous in nature, since the density of the fibers was larger near the mid-plain than in the surrounding areas. **Agarwal and Chaturvedi** [7] developed highly transparent composite materials. Their approach involved the matching of refractive indices of the glass fibers and matrix material as closely as possible. This was achieved by using two additives; **di-vinyl benzene** and **di-butyl pthalate** to alter the refractive index of polyester resin to the desired level. Fairly good results were achieved in this way .

The model materials developed by all of the above investigators had been successfully used in their investigations. However, it is desirable that isoclinics and isochromatics

obtained from such models be still sharper for more accurate analysis. The problem becomes even more acute for dynamic fracture analysis. It is for this reason that an improvement in the optical properties of model material was undertaken. Such an objective can only be met by understanding the behaviour of light as it passes through a non-homogenous media, such as a composite laminate.

2.3 Optical Considerations for a Model Material:

In section 2.1, various properties required for a good orthotropic material have been discussed. Of these, the first two conditions can be satisfied by controlling various parameters related to material processing. What follows are details of how various requirements for arriving suitable model material can be met.

2.3.1 Transparency:

The transparency of a model material depends on:

1. **Transparency of matrix material:** The matrix material should be transparent. Fortunately, most of the epoxy and polyester resins, which are transparent and are been extensively used for photoelastic analysis of isotropic materials, can also be used as matrix materials.
2. **Matching of Refractive Indices of Matrix and Fibers:** The refractive indices of matrix material and glass fibers affect the transparency of the composite significantly. Severe optical inhomogeneity (caused due to mismatch between refractive index of glass fiber and matrix

material) can render an otherwise good model material useless in two ways. Firstly, the loss transparency occurs due to scattering of light at the fiber-matrix interface. Consequently, the model material becomes opaque or turgid.

Another optical phenomena, which is more detrimental than the loss of transparency in model material for photoelastic application, is due to differential refraction of light passing through an optically inhomogeneous system. The effect of Snell's Laws of Refraction may be illustrated by considering the path of light as follows:

Consider that a parallel beam of light is incident on a body which has two parallel faces. The body may be:

1. Optically homogeneous (Fig. 2.1-a).
2. Having two different materials which have different refractive indices and an interface plane parallel to external surface on which light is incident (Fig. 2.1-b).
3. Having solid medium with a solid inclusion which has a curved external surface (Fig. 2.1-c).

In the first case, all rays of incident and emergent beam will be collinear and mutually parallel. In the second case, the angle of deviation for each ray in a particular medium will be the same. However, this angle of deviation will vary from medium to medium. Further, in this case, the emergent rays will be mutually parallel, subject to the restriction that incident rays are

parallel. In the third case, the situation is entirely different. Here, different rays will deviate by different angles. Hence, the **emergent rays will not be parallel.**

In glass fiber reinforced materials, glass phase is uniformly dispersed in the matrix material in the form of thin circular cylinders. Hence, the cross-section of a composite plate containing a single glass fiber can be represented as depicted in Fig. 2.1-c. However, in actual systems, there are a number of such **cylinders.** Consequently, a beam of light emerging through such a composite plate will be of a highly dispersed and diffused nature. Thus, even a slight mismatch in the refractive indices of glass fiber and matrix reduces the suitability of composite plate for photoelastic purposes appreciably. Therefore, the first challenge to produce a superior photoelastic orthotropic model comprises of matching the refractive indices of glass fiber and matrix as closely as possible.

3. Presence of Entrapped Air: Any air bubbles if present in the matrix phase, lead to same problems as does the mismatch between the refractive indices of glass fiber and matrix. Hence, it is very important to remove any air which gets entrapped in the laminate. One method to remove these bubbles is by curing the resin in vacuum.

The affect of the presence of glass fibers in a composite model material on the path of light was studied in great detail by **Agarwal and Chaturvedi** [7]. They found out that:

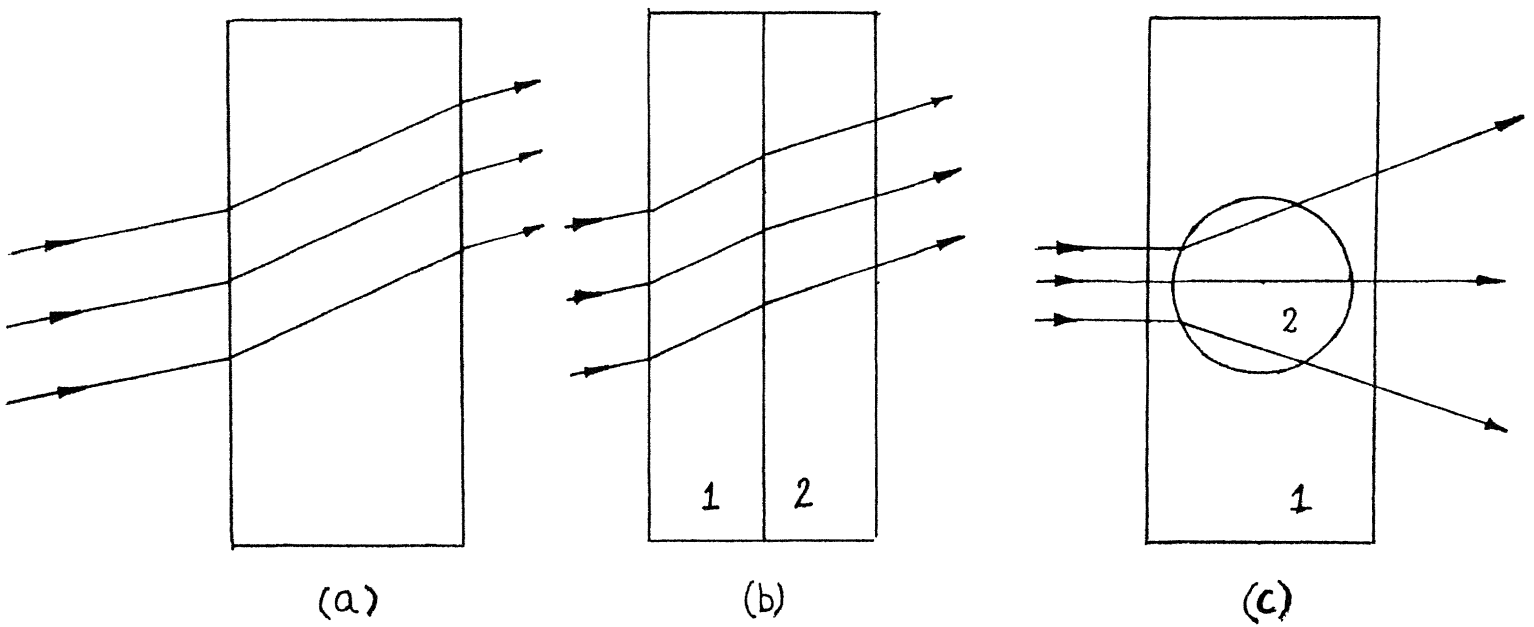

Fig. 2.1: Schematic representation of light through (a) Homogenous solid (b) Two solid mediums with a straight interface (c) Solid medium with another inclusion having a curved interface.

1. A parallel beam of light appears smeared in the direction perpendicular to the fibers.
2. Sharp boundaries of an object, when viewed through the model, appear smeared again in the direction perpendicular to the fibers. As a consequence, very closely spaced straight and parallel lines do not appear distinct.

These two effects, the investigators concluded, cause a reduction in the sharpness of isoclinic and isochromatic fringes. Hence, an orthotropic photoelastic model is superior when it is:

1. Highly transparent.
2. Causes minimum distortion of the view of an object when seen through it.

2.3.2 Homogeneity and Orientation of Fibers:

The properties of model material should be same at all the points in the body. Another requirement for a satisfactory model material is that the orientation of fibers should be as exact as desired. Both these conditions will also ensure the reproducibility of the results.

2.4 Fabrication of the Model:

As discussed earlier, the two most significant considerations for obtaining optically superior composite model materials constitute matching of the refractive indices of fiber and matrix and removing any air which gets entrapped.

To achieve these ends, various combinations of matrix material and glass fibers were tried.

2.4.1 Selection of Glass Fiber:

Among glass fibers; both, glass roving and unidirectional mat were tried. There specifications are:

1. **Unidirectional Glass Fiber Mat:**
   Manufacturer : Fothergill Engineered Fabrics Ltd., U.S.A
   Style : 12ØØ Tex, 4 Threads per cm.
   Area Density : 5ØØ gm./mm^2
   Type : Unidirectional plain
   Width : 5Ø cm.

2. **Glass Roving:**
   Manufacturer : Ceat Ltd., Glass Fiber Division, Hyderabad
   Style : 3ØØ Tex
   Brand : DR 6ØØ FE
   Size : Each spool of 4.Ø Kgs.

Not much success was achieved with glass rovings. The principal reason for this was poor penetration of resin compounded with poor wetting of fibers. Problems encountered with the usage of unidirectional glass fiber mat were of a different nature. In this case, there was little problem as far as penetration and wetting was concerned. However, using glass fiber mat as it is, led to opacity in some zones of the laminate. This was due to the presence of thick pre-impregnated bundles of glass fibers in warp and weft directions at these locations. These fiber-bundles have been introduced in the mat by the manufacturers to maintain the orientation of glass fibers.

In light of these observations, it was realized that glass fiber mat is preferable over glass roving. It was further realized that the model material developed from unidirectional mat will be perfect only if the "thick bundle of prepreg fibers" could in some way be removed from the mat.

2.4.2 Selection of Matrix System:

Four grades of matrix materials were tried. They were:

1. Epoxy resin (LY-5Ø52) and hardener(HY-5Ø52) manufactured by Hindustan Ciba Geigy Ltd., Bombay.
2. GP (general purpose) polyester resin manufactured by Parikh Chemicals Ltd., Kanpur.
3. Clear Casting Grade Polyester Resin manufactured by Parikh Chemicals Ltd., Kanpur.
4. Polyester resin having mono-maleic acid (MMA) monomer.

Each of these resins was used with glass roving as well as glass fiber unidirectional mat. In addition, suitable silane coupling agents were also used in these matrix-systems. The influence of silane coupling agents was **not dramatic**. However, wetting improved to some extent in cases where glass roving was used.

Wetting and penetration were good enough in case of epoxy resin. However, problems encountered with this resin were:

1. The colour of matrix material after curing was dark yellow; which is not preferable.
2. The time required for the resin to solidify was not large. A longer curing time is helpful in removal of entrapped air bubbles, when casting occurs in vacuum.

The advantages of clear casting grade polyester resin were its low viscosity and colorless complexion. However, the difference in the refractive indices of fiber and matrix was found to be so large that it was not considered worthwhile to work with this resin system. Similar problems were also encountered when polyester resin having MMA polymer was used.

General purpose polyester resin was found to be the most suitable resin. Its refractive index was very close to that of glass fiber. The small difference between refractive indices of fiber and matrix was further minimized by adding 1Ø% styrene by weight.

2.4.3 Fabrication Procedure for the Model Material:

Initially the ends of the fibers were bound using epoxy resin. For this purpose, epoxy resin (LY556) and hardener (HY951), manufactured by Hindustan Ciba Geigy Ltd. were used in the ratio of 1Ø:1 respectively. Such a **pre-treatment** process was "essential", since in the absence of this treatment, the alignment of the fibers gets disturbed while treating the mat for removal of pre-preg fiber bundles. The relevant details of pre-treatment procedure are shown in Fig. 2.2.

Next, the matrix material was prepared. For this purpose, GP polyester resin was used. This resin has a low viscosity. Methyl ethyl ketone peroxide (MEKP) was added as 1.Ø percent of the weight of resin to act as catalyst. 1.Ø percent cobalt octate (by weight) was used as accelerator. The resin was heated in a temperature controlled oven to ensure the removal of traces of water droplets, present if any. It was also ensured that accelerator was added to resin after the addition of catalyst. These two chemicals were mixed uniformly in the resin.

Pre-treated unidirectional glass mat was cut in pieces of desired size. Next, each piece of mat was soaked in resin. Care was taken to minimize the amount of air entrapped at this stage. Hence, resin was spread on the mat with a rubber lined roller,

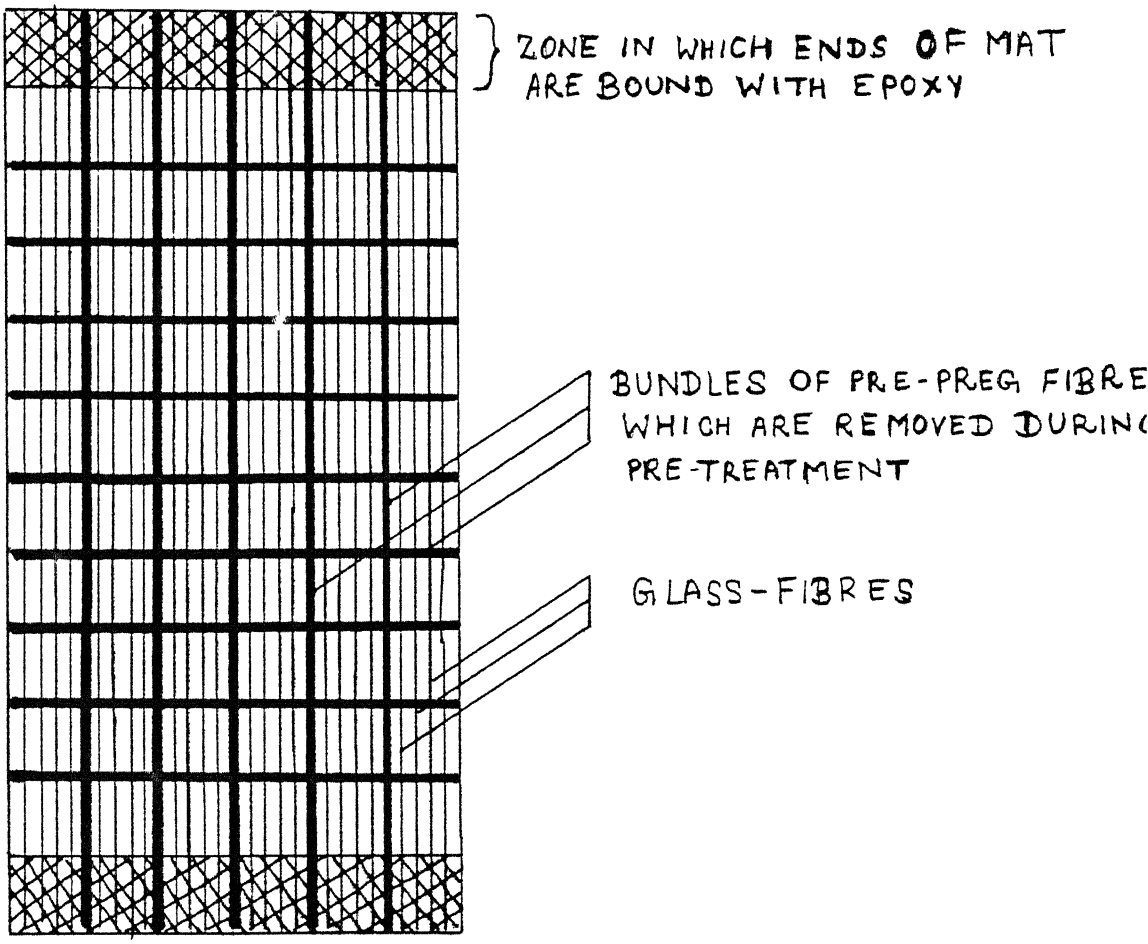

Fig. 2.2 Zone in which epoxy resin is to be applied for Pre-Treatment process.

instead of a brush. Once the mat was fully wet, bundles of pre-impregnated fibers were removed using a pair of tweezers. Removal of pre-preg fiber bundles is possible only when the fibers are in a wet state, since the adhesive which binds pre-preg fibers to the mat, gets dissolved in polyester resin or styrene or acetone. A parallel attempt was made to remove these pre-preg fibers and then applying acetone or styrene to the mat, followed by drying the mat in oven, and then using the mat for casting purposes. However, not much success could be attained in this direction since the application of styrene or acetone led to the removal of 'size' from the surface of glass fibers and hence caused poor wetting.

In this way, several layers of glass fibers were stacked up, and covered with mylar sheet on both sides. The entire set up was placed between two perspex plates separated by 3 mm. thick aluminium spacers, as shown in Fig. 2.3.

Next, the fibers were subjected to tension to ensure proper alignment of the fibers. This was done by clamping the ends of the fibers by a steel plate and adjusting the position of the tension screw (Fig. 2.3). This was followed by clamping the perspex plates by nuts and bolts. An interval of 5-10 minutes was given to facilitate the flow of extra resin out of the mold,due to clamping pressure. Later, the tension in the fibers was removed and the entire setup was subjected to vacuum pressure for approximately five hours to ensure the removal of air bubbles. This was followed by curing the resin at 60 ^{o}C for 12 hours followed by postcuring the laminate at 80 ^{o}C for six hours.

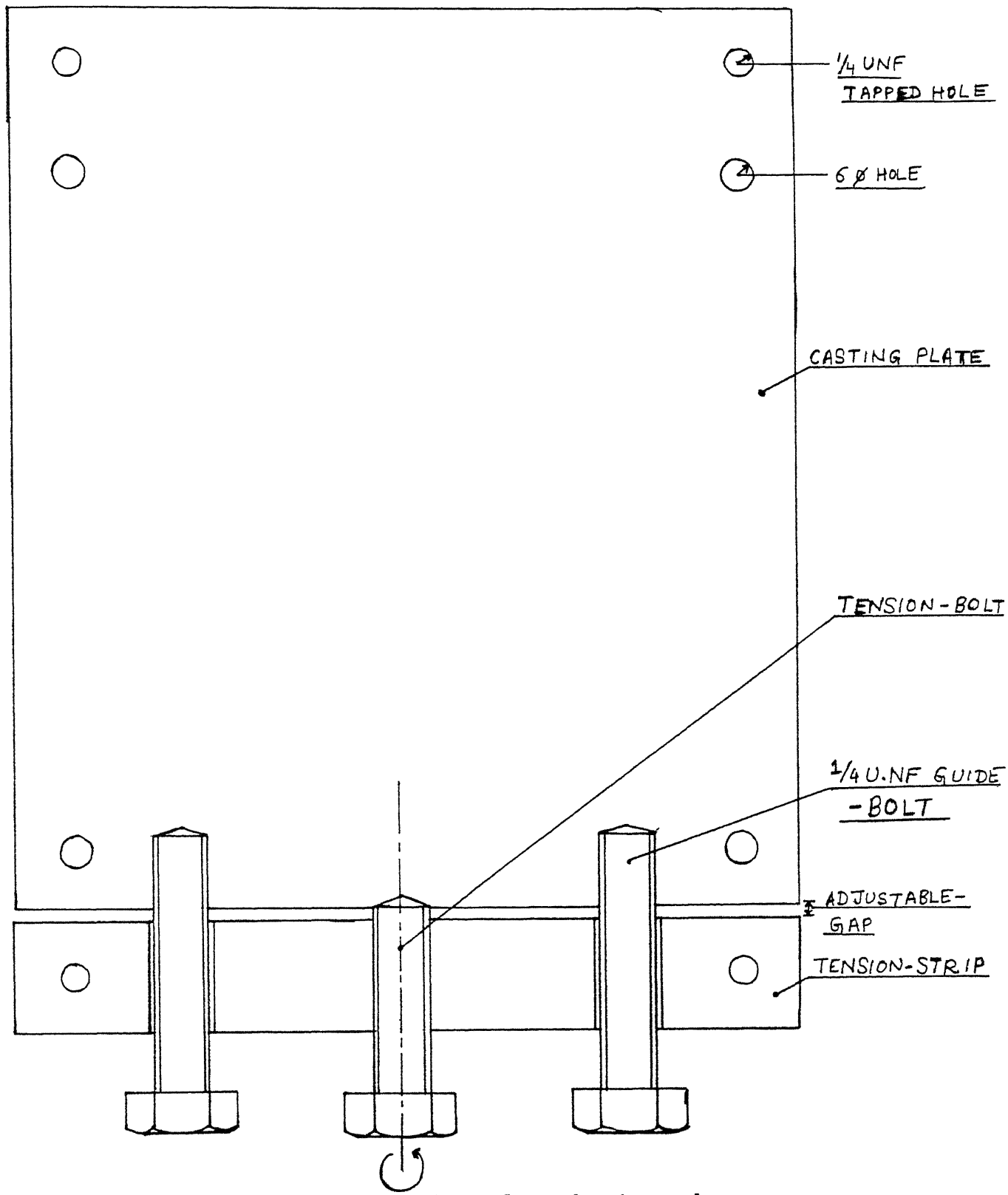

Fig. 2.3 Diagram of casting plate having features to subject fibers to tension.

2.5 Optical Properties of Model Material:

Optical properties of unidirectional composite model material was examined to assess the suitability for photoelastic analysis and allied applications. The model material has been tested for transparency, resolution of closely spaced lines and photoelastic effect. The relevant details follow:

2.5.1 Transparency:

The transparency of the model material developed was assessed in terms of **transmission ratio**. Transmission ratio is defined as the ratio of incident light's intensity to that of emergent light.

The circular disc model was placed in the path He-Ne Laser beam. The emergent beam was focussed, using a convex lens , on the sensing element of the photometer. Intensities of the emergent and incident beam were measured using a digital photometer. The entire setup is shown in Fig. 2.4. The value of transmission ratio for the model material (3.2 mm thick) developed was found to be Ø.69 and was greater than that for the model material developed by **Chaturvedi** [8] which had a transmission ratio of Ø.58.

2.5.2 Resolution of Lines Through the Model Material:

It has been discussed in the preceding passages that the sharp boundaries of an object appear blurred when viewed through a composite model whose constituents do not have well matched refractive indices. This effect was examined by viewing closely spaced straight and parallel lines through the models. Two sets

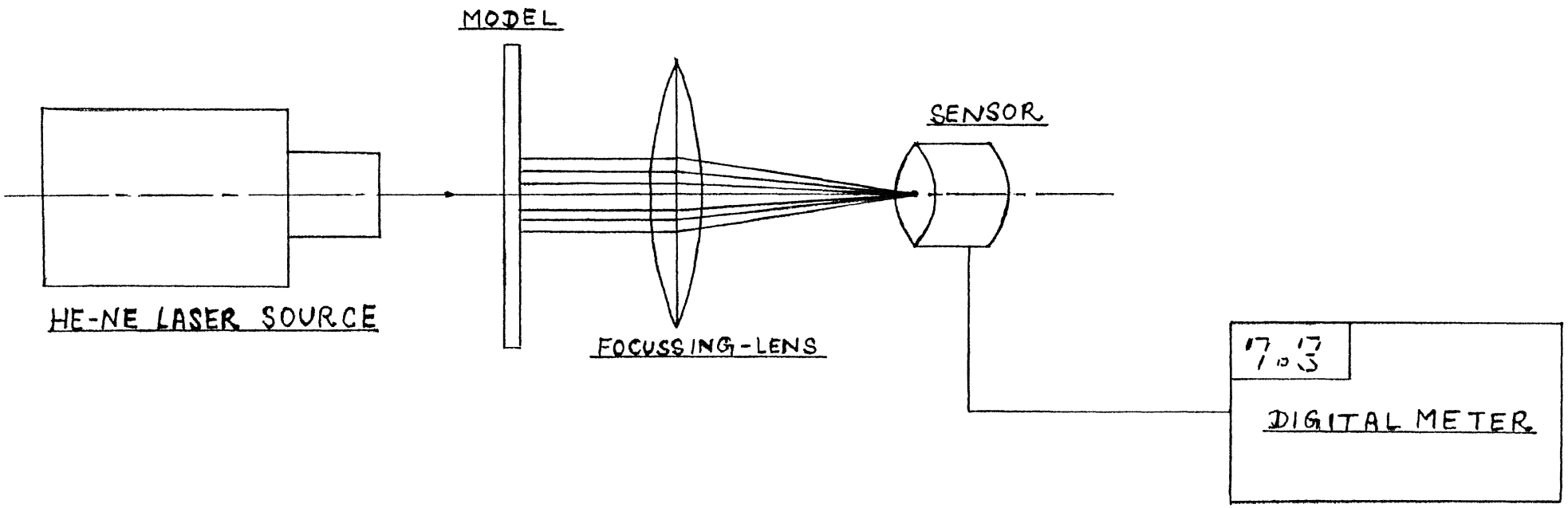

Fig. 2.4-a: Schematic layout of experimental setup used for the determination of transmission ratio of the model material.

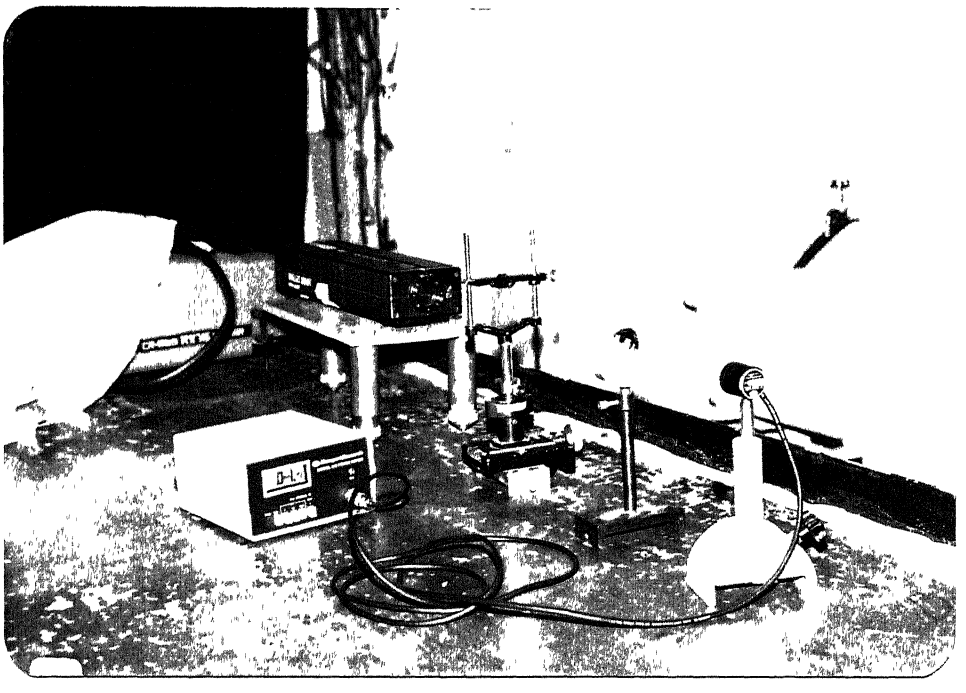

Fig. 2.4-b: Photograph showing experimental setup for the determination of transmission ratio of model material.

of equispaced lines were drawn inside a circle with lines in one being perpendicular to those in the other set (Fig. 2.5-a). These lines were viewed through through circular discs of unidirectional model material (Fig. 2.5-b). Direction of the fibers has been indicated by arrows in the figure. It is clear from the figures that the lines are distinguishable from one another. Placing an optically inferior model over such a set of lines revealed that lines which were parallel to the fibers appeared blurred.

2.5.3 Photoelastic Effects:

The model materials have been examined for photoelastic effect by placing their circular disc models in a circular polariscope employing a diffused sodium light source. The discs were loaded in diametral compression with fibers oriented at 90° to the loading axis. The resulting fringe patterns for unidirectional models have been shown in Figs. 2.6-a and 2.6-b, the latter pertaining to an inferior model material.

It is amply clear from the figure that the fringes for superior model material are much better defined than for other material (Fig. 2.6-b). Some nonuniformity of fringes parallel to fibers occurs due to non uniform distribution of fibers. For this reason the photoelastic sensitivity of the model material varies from point to point.

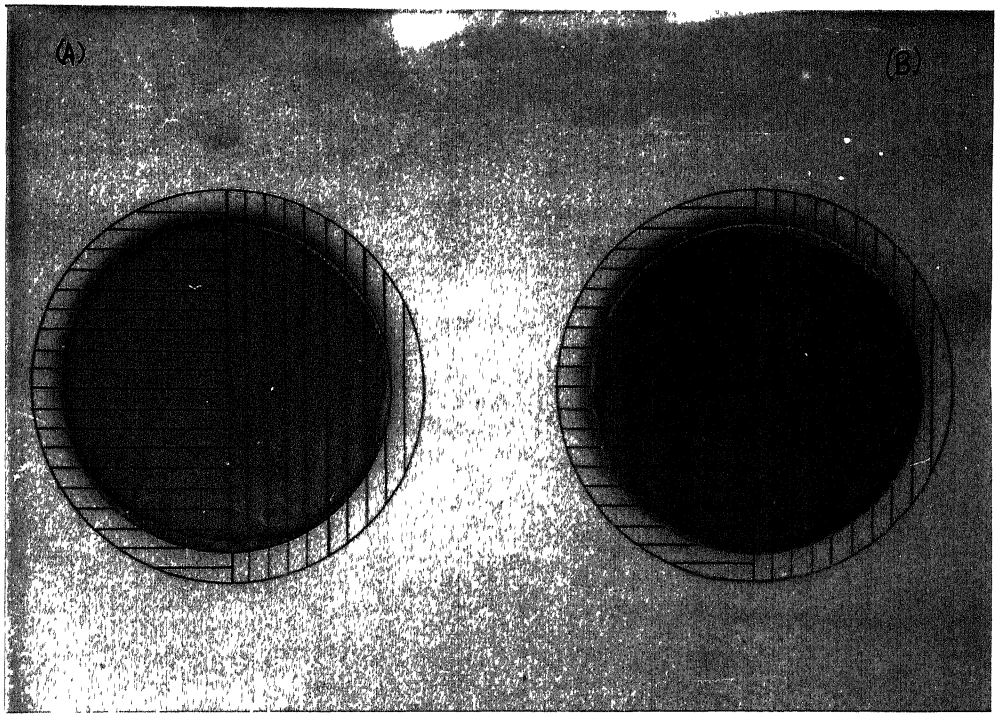

Fig. 2.5: View of parallel lines through a;
(a) Superior model material.
(b) Model with larger mismatch of refractive indices.

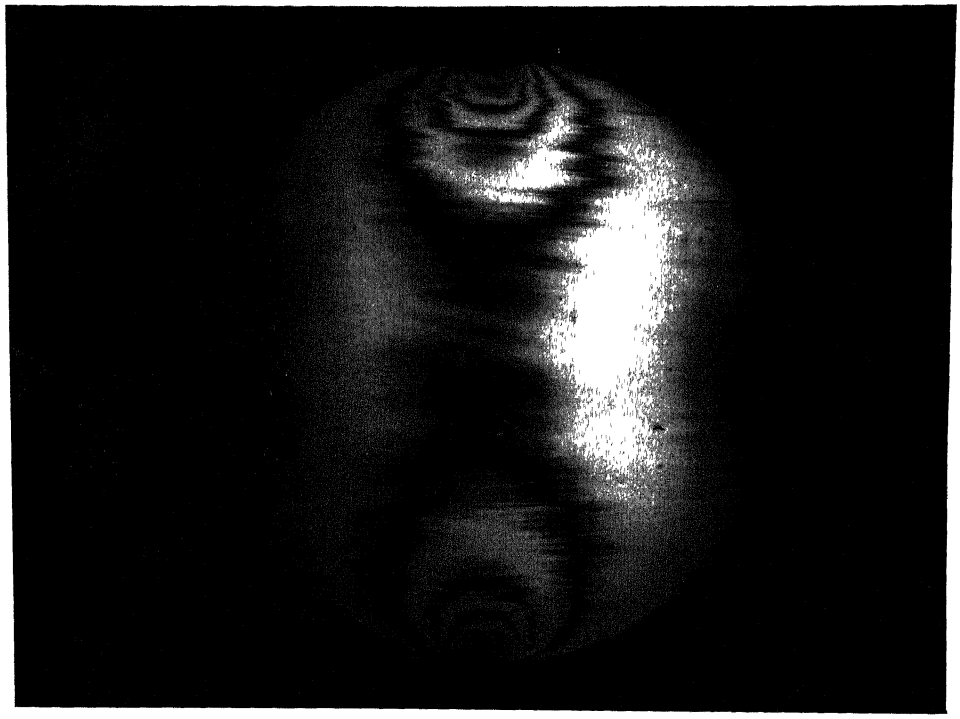

(A)

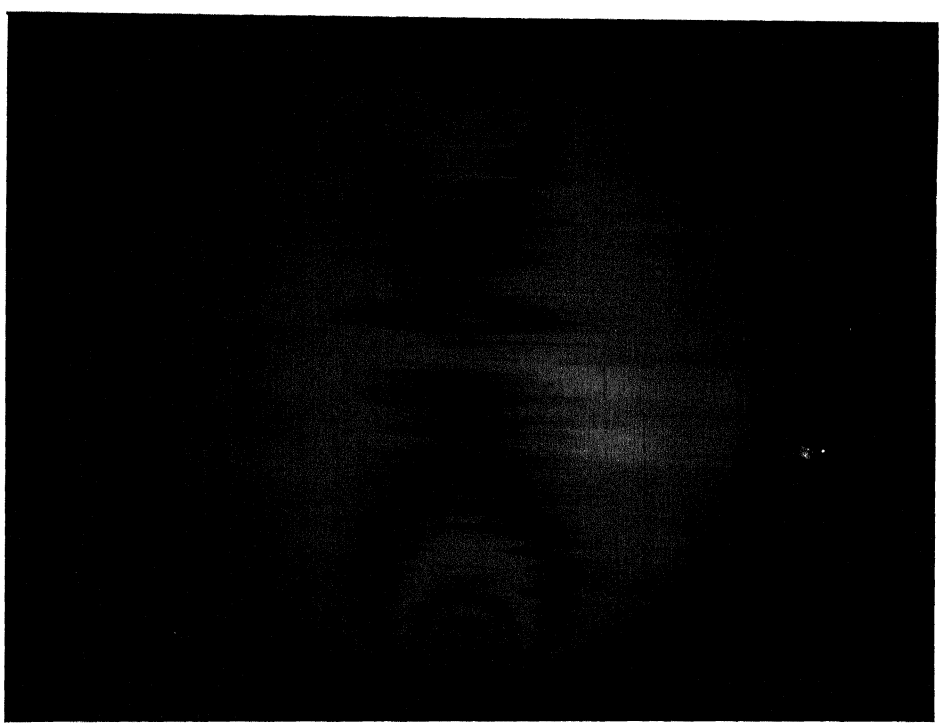

(B)

Fig. 2.6: Isochromatic fringe patterns for;
(a) Superior model material.
(b) Model with large mismatch of refractive indices.

3 COMPOSITE CHARACTERIZATION :

3.1 Introduction:

Any material, when newly developed needs to be fully and accurately characterized before it can be put to other uses. This necessity becomes all the more important for composite materials, since their properties depend on a large number of parameters. In the present investigation, the newly developed material was tested for its mechanical and photoelastic properties. The former included elastic constants and Poisson's ratio and elastic constants, while the latter included three stress-optic coefficients.

3.2 Experimental Setup :

While fabricating the model material it was felt that the process of fabrication is very tedious and time consuming. For this reason, it was natural to design and develop a suitable experimental setup to ensure:

1. That the material be characterized accurately.
2. The amount of model material consumed is minimum.

The available infrastructure in the laboratory included a MTS machine (suitable for mechanical characterization) and a polariscope cum loading frame (suitable for photoelastic characterization). One option available, was to use these two facilities separately for their respective purposes. However, this was later found to be unfeasible due to the following reasons:

1. The material developed seemed to a have very high value of stress optic coefficient in the longitudinal direction ($F_{\sigma L}$). This in turn meant that very large loads were needed to produce appreciable photoelastic effect in the material. However, the conventional loading frame available was not found to be strong enough to bear such high loads.
2. A procedure for characterizing the model material separately for its photoelastic and mechanical properties required larger amount of model material an time.

In light of the above constraints, it was decided to develop a new setup which could suffice the following conditions:

1. It was rigid enough to take high loads.
2. It incorporated certain features which could facilitate photoelastic as well as mechanical characterization of the model material simultaneously.

The new setup comprised of the MTS machine having a quarter wave plate and a polarizer on its one side and an analyzer along with another quarter wave plate on its other side. A light box having white and sodium light sources was kept behind the polarizing element. While arranging the polariscope's elements on either side of the MTS machine it was ensured that surface of the tension test specimen when loaded on the MTS remained parallel to the optical elements and also that the light coming from the light box was incident normally on the specimen. Such an alignment between the specimen, elements of polariscope and light box was maintained by using a try-square. This was very important

since laws of photoelasticity are valid as long as the angle of deviation of a light ray passing through the specimen is zero.

3.2.1 Material Testing System:

The Material Testing System (model MTS 810) is a servo-hydraulic testing system designed with a view to accommodate a wide variety of standard material tests. The testing machine has the load range capacity of -100 kN to +100 kN which can be applied in the form of a sine, ramp, haversine, triangular and other programmable waveforms. It uses a microconsole (458.20) to provide closed loop control of the servo-hydraulic system. Specimen is gripped in the load unit. Hydraulic power supply is linked to the microconsole. To control the tests, microconsole has a Displacement AC controller, Load DC controller and Strain DC controller. Testing can be done in any of these control modes. To generate a waveform microconsole, has a microprofiler which can be operated in three modes viz. programmed, direct and remote. This machine can perform Tensile, Fatigue and some other type of tests.

The entire setup has been schematically illustrated in Fig. 3.1. A photograph of the setup is shown in Fig. 3.2.

With the aid of such a setup, it was possible to record the following information during the tension test:

1. The external load on the specimen. This was accomplished by using a load-cell having a maximum load rating of 10 kN.

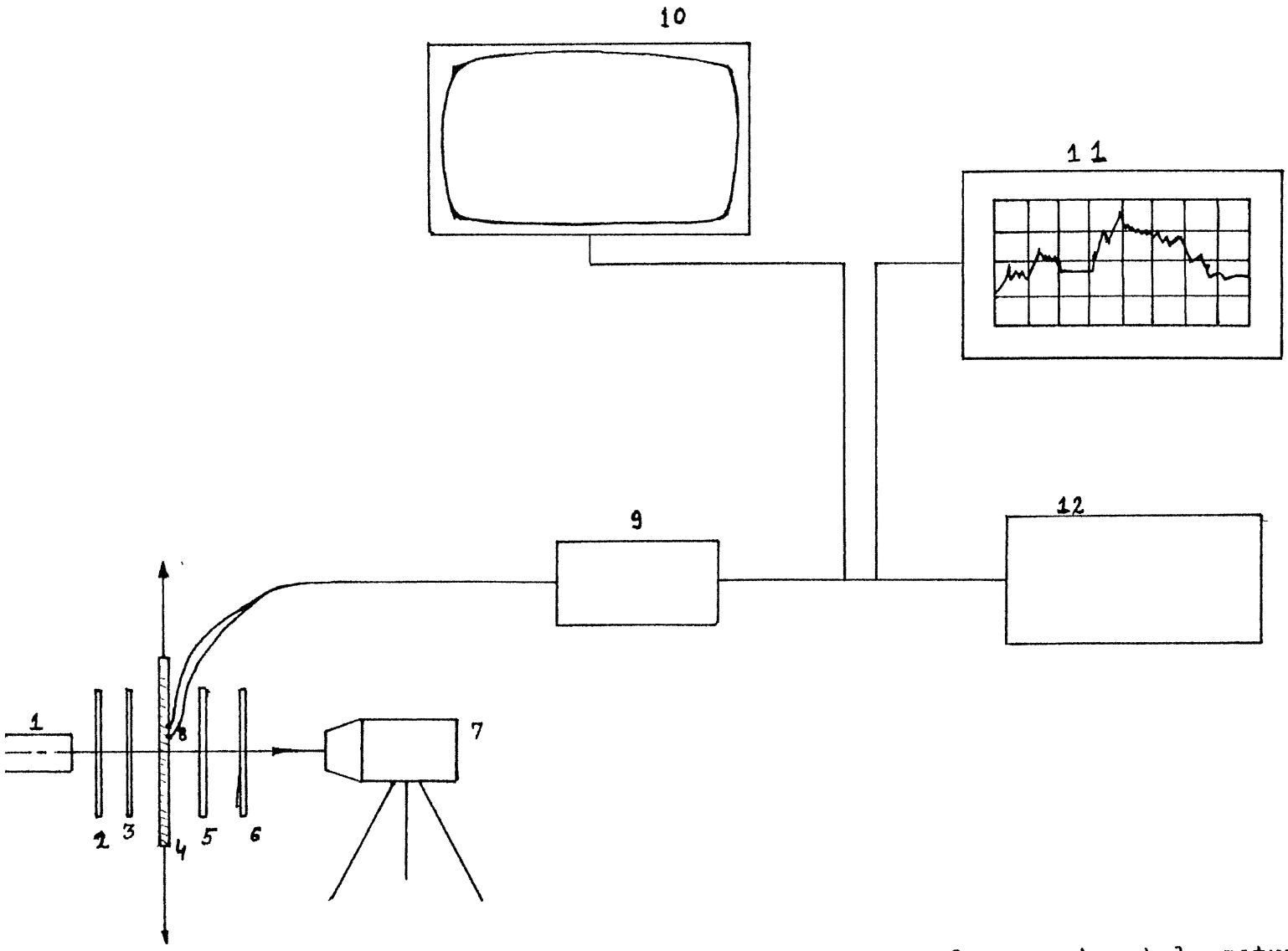

REFERENCE	
No	DESCRIPTION
1	LIGHT SOURCE
2	POLARIZER
3	QUARTER WAVE PLATE
4	SPECIMEN
5	QUARTER WAVE PLATE
6	ANALYZER
7	CAMERA
8	EXTENSOMETER
9	INTERFACE
10	PC - MONITOR
11	PLOTTER
12	CONSOLE

Fig. 3.1 Schematic layout of experimental setup developed for material characterization.

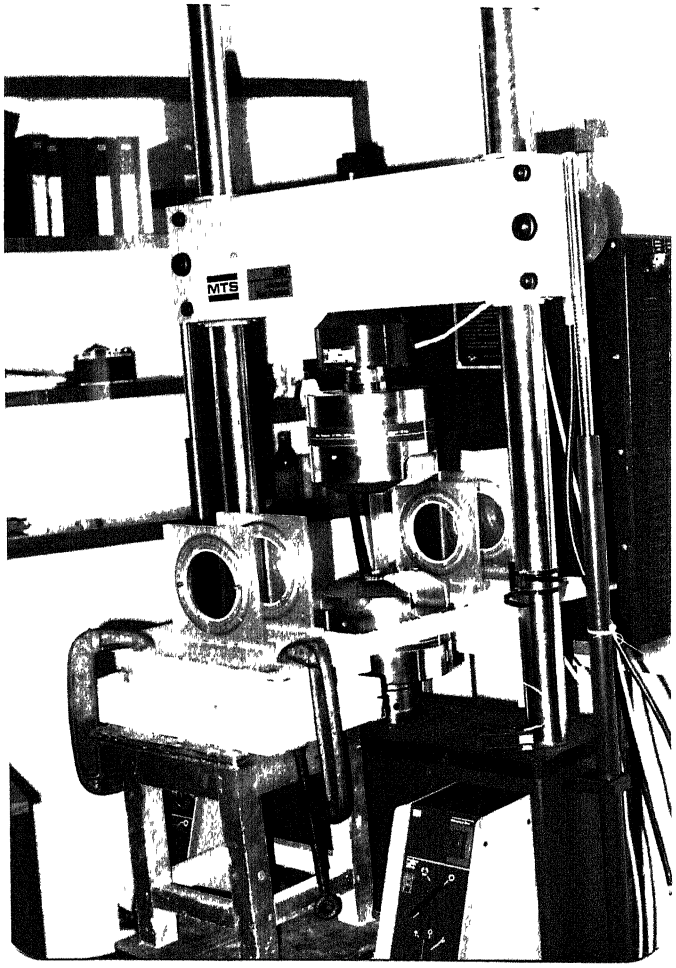

Fig. 3.2: Photograph of experimental setup prepared for material characterization.

2. The strain at any desired point on the specimen. This could be found out by using an extensometer meant for measuring longitudinal strains.
3. The photoelastic response of the material in terms of the fringe order at the point of interest. For recording the fringe order, monochromatic sodium light was used. White light was not preferred since the ordering of fringes for such a light is very difficult. This is so, since the colour of fringes changes appreciably with respect to change in fringe order . Hence, recognition of these colours depends heavily on human judgment, which can introduce very large errors.

From this information, extensional elastic moduli and stress-optic constants for any particular direction could be evaluated simultaneously.

By testing samples with fiber orientation at 0°, 90° and 45°, the values of E_L, E_T, E_{45}, F_L, F_L,F_{45}, were found out. However for the evaluation of shear modulus (G_{LT}) and Poisson's ratio (ν_{LT}), lateral strains were needed. These strains were measured by using lateral extensometer. The setup of lateral extensometer is shown in Fig. 3.3.

3.3 Mechanical Characterization :

The volume fraction of fiber the for model material has been calculated as follows:

Thickness of the specimen = 3.2 mm.

Density of glass fiber = 2.54 gm./cc

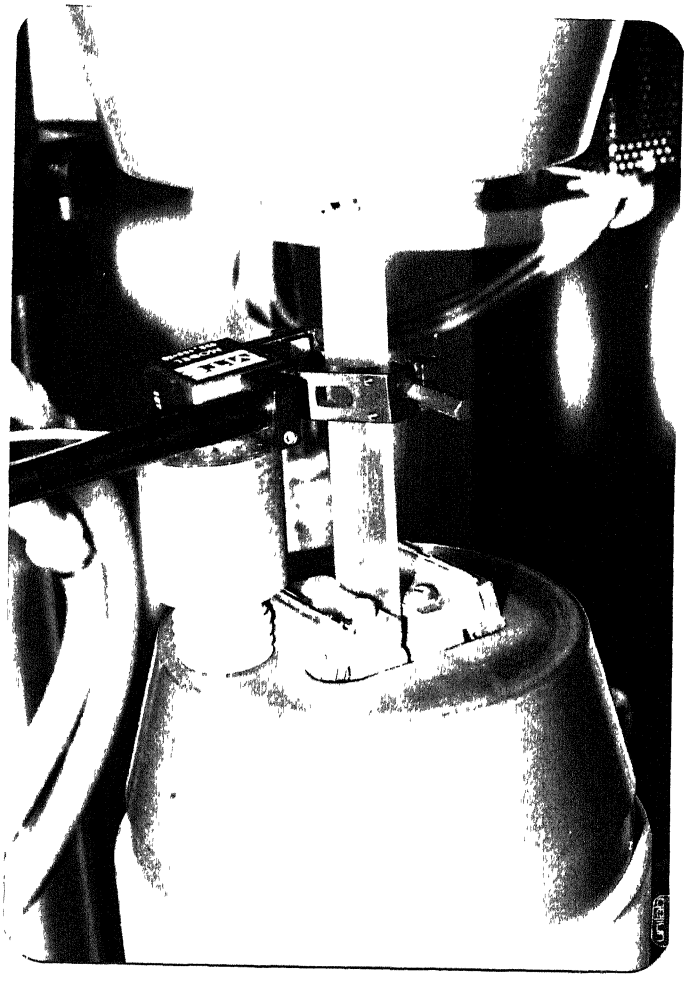

Fig. 3.3: Photograph showing the setup of diametral extensometer for the measurement of lateral strains.

Area density of the mat = 405.0 gm. per sq. m

No. of layers in each laminate = 7

For 1 m^2 of laminate, volume of glass= 405•7/2.54 = 1116.1 cc

Volume of laminate = 3200 cc.

Volume fraction of fiber = 1116.1/3200 = 34.88 %

Other properties which were required for the model material are :

1. Extensional modulus in the longitudinal direction (E_L).
2. Extensional modulus in the transverse direction (E_T).
3. Poisson's ratio (ν_{LT}).
4. Shear modulus (G_{LT}).

For evaluation of these properties the following relations can be used:

$$E_x = \sigma_x/\epsilon_x \qquad \text{when } \sigma_y = 0,\ \tau_{xy} = 0 \qquad (3.1)$$

$$\nu_{xy} = -\epsilon_y/\epsilon_x \qquad \text{when } \sigma_y = 0,\ \tau_{xy} = 0 \qquad (3.2)$$

$$G_{LT} = \sigma_x/[2(1+\nu_{xy})] \qquad \text{when } \sigma_y = 0,\ \tau_{xy} = 0,\ \sigma_x = \sigma_{45^\circ} \qquad (3.3)$$

Using Eq. (3.1), elastic moduli (E_L, E_T) can be easily evaluated. Eqs. (3.2) and (3.3) can be employed to find out the Poisson's ratio (ν_{LT}) and shear modulus (G_{LT}) respectively.

For the calibration of the model material, static uniaxial tension tests were carried out on flat specimens with rectangular cross-sections. While conducting the tests, the strains in the longitudinal and lateral directions were recorded along with the applied loads. The details of the experimental setup have been given in section 3.2.

By conducting uniaxial tension tests for 0° and 90° samples, E_L, E_T and ν_{LT} were evaluated. For finding G_{LT}, an off-axis 45° coupon test was conducted, and using Eq. (3.3) G_{LT} was computed.

While conducting the test in the longitudinal direction, it was ensured that the direction of application of load coincided with the material direction of the orientation of the fibers. This is very important since the gradient of elastic modulus in θ direction (E_θ) with respect to orientation of external load (i.e. $dE_\theta/d\theta$) is very high near $\emptyset^\circ$.

3.3 Photoelastic Characterization :

3.3.1 Assessment of Existing Theories of Photo-Orthotropic Elasticity:

A polarized study of glass fiber laminates by **Horridge** [9] seems to be the first attempt in the direction of photoelastic application to reinforced plastics. **Pih and Knight** [2], proposed a stress optic law for transparent composites. They also observed that isoclinics are not representatives of the principal stress directions.

$$F_{\sigma\theta} = \sigma \cdot t/N_\theta$$

However their stress-optic law, based on the concept of average optical behaviour and involving a single photoelastic constant for orthotropic materials, was unrealistic.

Sampson [3], using the analogy of the Mohr's circle for stress suggested an equivalent circle for birefringence. He postulated that orthotropic materials can be characterized with three principal stress values $F_{\sigma L}$, $F_{\sigma T}$, $F_{\sigma LT}$, and that the stress system σ_L, σ_T, τ_{LT} produces three components of birefringence which are defined as:

$$N_L = \sigma_L/F_{\sigma L} \qquad (3.4\text{-a})$$

$$N_T = \sigma_T/F_{\sigma T} \qquad (3.4\text{-b})$$

$$N_{LT} = 2\cdot\tau_{LT}/F_{\sigma LT} \qquad (3.4\text{-c})$$

where the subscripts L and T refer to principal material axes. The resultant birefringence is:

$$N = [\{\sigma_L/F_{\sigma L} - \sigma_T/F_{\sigma T}\}^2 + \{2\cdot\tau_{LT}/F_{LT}\}^2]^{\frac{1}{2}} \qquad (3.5)$$

Dally and Prabhakaran [4] refined the stress proportioning method used by **Pih and Knight** [2], to derive another stress-optic law. Their formulation was governed by the following equation:

$$N = N_{matrix} + N_{fibers} \qquad (3.6)$$

From Eq. (3.6), the authors established equivalence between the values of F_θ as predicted by their theory and that by Eq. (3.5). This is given in Eq. (3.7).

$$(F_{\theta Prabhakaran})^2\cdot(1+\cap) = (F_{\theta Sampson})^2 \qquad (3.7)$$

where $\cap$ is a difference term.

It was found by these investigators that the maximum value of $\sqrt{(1+\cap)}$ was 1.Ø6 when θ assumed a value of 28 deg. Thus if the difference term in Eq. (3.7) is neglected, since it is very small, then then the formulation of Sampson's and Prabhakaran's are identical. However, these investigators did not discuss the physical significance of the isoclinics.

Bert [14] assigned tensorial nature to birefringence on the basis of crystal theory of **Bhagavantham** [15]. By relating a second order birefringence tensor to second order stress tensor through a fourth order photoelastic-property tensor, Bert formulated a stress-optic law. However, his relations were not simple enough to be used in experiments. Besides this, Bert did not corroborate his predictions by experimental evidence.

Pipes and Rose [6] proposed that strain-optic laws could only be employed for composites with low volume fraction of fibers and verified their contention experimentally. Further, they developed a strain-optic law by assuming that birefringent composite materials obey the classical strain-optic relations for isotropic materials. For unidirectional fiber composites,the strain-optic law proposed by them was:

$$\epsilon_1 - \epsilon_2 = n \cdot f_\epsilon / t = N \cdot F_\epsilon \qquad (3.8)$$

In Eq. (3.8), subscripts 1 and 2 indicate the direction of principal strains and F_ϵ is the strain-optic coefficient. A novel feature of their law is that it requires only one material constant. However this relation can not be used for composites having large fiber content.

Agarwal and Chaturvedi [7] have assessed various theories of photo-orthotropic-elasticity on the basis of an extensive work conducted on 'superior' model materials developed by themselves. They have shown that the isoclinics are closer to the contours of principal strain differences rather than those for principal stress differences. This very important observation prompted **Agarwal and Chaturvedi** [16],to derive a general strain-optic law. This derivation was mathematically sound. Their exact strain-optic law based on **Bhagvantham's** [15] theory of crystalline photoelasticity is:

$$N = \left[\{\epsilon_L/F_{\epsilon L} - \epsilon_T/F_{\epsilon T}\}^2 + \{2 \cdot \gamma_{LT}/F_{\epsilon LT}\}^2\right]^{1/2} \qquad (3.9)$$

$$\mathrm{Tan}2\phi = [\gamma_{LT}/F_{\epsilon LT}] \div [\epsilon_L/F_{\epsilon L} - \epsilon_T/F_{\epsilon T}] \qquad (3.10)$$

where;

N = Fringe order

ϕ = Isoclinic angle

F = Strain-optic coefficient

y = Shear direction

ϵ = Extensional strain

L,T ≡ Refer to longitudinal and transverse directions

Further, these investigators realized that the degree of orthotropy with respect to strain-fringe value is considerably smaller than with respect to stress-fringe value. This finding prompted the investigators to conclude that an approximate strain-optic law was likely to introduce much smaller errors than an approximate stress-optic law. On the basis of this intuition, they proposed an approximate law to estimate the direction of principal strains and also to predict the values of principal strain difference at a point. It was found that the error introduced by such an approximate law was small enough and within the experimental limits.

$$N = [\{\epsilon_L - \epsilon_T\}^2 + \{2 \cdot y_{LT}\}^2]^{1/2} \div F_\epsilon \qquad (3.11)$$

$$\text{Tan}2\phi = y_{LT} \div [\epsilon_L - \epsilon_T] \qquad (3.12)$$

Agarwal [17] proposed another approximate strain-optic law which was much more accurate than as given in Eqs. (3.11) and (3.12). This law was obtained by approximating the ratio $(F_{\epsilon L}/F_{\epsilon T})$ to unity on the basis of experimental evidence. The resulting modified law becomes:

$$N = (\epsilon_L - \epsilon_T) \cdot [\cos^2 2\theta + (F_{\epsilon L}/F_{\epsilon LT})^2 \cdot \sin^2 2\theta]^{1/2} \div F_L \qquad (3.13)$$

$$\text{Tan}2\phi = (F_L/F_{LT}) \cdot \text{Tan}2\theta \qquad (3.14)$$

With so many theories available, each varying in its accuracy and approachability, it required sound judgment to choose the most appropriate one of these for further investigations. Two considerations which governed the selection

of such a theory were:

1. Accuracy of the theory.

2. Ease in usage of the selected photo-orthotropic law.

In light of these two constraints, it was realized that the determination of three stress-optic constants ($F_{\sigma L}$, $F_{\sigma T}$, $F_{\sigma LT}$) as proposed by Sampson for the model material would suffice our purpose. These three constants are defined as under:

$$F_{\sigma L} = \sigma_L \cdot t/N_L \tag{3.15}$$

$$F_{\sigma T} = \sigma_T \cdot t/N_T \tag{3.16}$$

$$F_{\sigma \theta} = \sigma_\theta \cdot t/N_\theta \tag{3.17}$$

$$F_{\sigma LT} = [(1/f_{\pi/4})^2 - \emptyset.25 \cdot (1/f_T - 1/f_L)^2]^{-\frac{1}{2}} \tag{3.18}$$

Thus, using Eqs. (3.15) and (3.16), $F_{\sigma L}$ and $F_{\sigma T}$ were evaluated, while Eqs. (3.17) and (3.18) were employed to find out $F_{\sigma LT}$ was evaluated. The exact fringe order at any point was found out by Tardy's method of compensation. The details of the experimental setup are given in the section that follows.

3.5 Analysis of the Collected Data:

3.5.1 Evaluation of Extensional Elastic Constants and Stress Optic Coefficients:

Currently, most of the investigators characterize a material with point-matching techniques. In such techniques it is assumed that materials behave in exactly the same way as predicted by mathematical models and thus the errors involved in the experimentation are not large. Thus very few data points are collected for analysis. Very little significance is attached to the amount of errors which may creep up in such an analysis.

These errors may be due to residual stresses, residual strains or various personal factors. This problem becomes all the more significant while calibrating the material for its photoelastic properties. In the present investigation, the method of least-square analysis was employed to filter out the error introduced due to various reasons during such characterization.

3.5.1.1 Linear Least Square Method :

Consider the following relations:

$$\sigma_i = E_i \cdot \epsilon_i \qquad (3.19)$$

$$\sigma_i = (1/F_{\sigma i}) \cdot (N_i/t) \qquad (3.20)$$

where;

σ_i = Externally applied stress along direction i

$F_{\sigma i}$ = Stress-optic coefficient for direction i

E_i = Extensional elastic modulus for direction i

N_i = Fringe order in the specimen for direction i

ϵ_i = Strain in i direction due to σ_i

Eqs. (3.19) and (3.20) can be generalized as:

$$S = M \cdot R \qquad (3.21)$$

where;

S = External stress

M = Material property

R = Response of the material (i.e. strain or fringe order)

If an additional constant term is added to the R.H.S of Eq. (3.21) to account for errors, then the said equation can be rewritten as:

$$g = y - a \cdot x + b \qquad (3.22)$$

For a perfect fit, g is zero. However, in other cases

Eq. (3.22) can be expressed in the matrix form as:

$$\{g\} = [c] \cdot \{z\} \qquad (3.23)$$

where;

{g} = Column vector for errors

[c] = Rectangular matrix having individual data points

{z} = Column vector for a and b as given in Eq. (3.11)

Using Eq. (3.23), the values of a and b can be evaluated as follows:

$$[c]^T \cdot \{g\} = [d]\{z\}$$

where;

$[d]$ = Square matrix $[c]^T \cdot [c]$

Thus;

$$\{z\} = [d]^{-1} \cdot [c]^T \cdot \{z\}$$

Using such an approach, extensional elastic moduli and photoelastic constants were evaluated. The values obtained were quite consistent with those mentioned in the available literature. The plots between stress and strain and between stress and fringe number for 0°, 90° and 45° are shown in Figs. 3.4, 3.5 and 3.6 respectively.

3.5.2 Determination of Poisson's Ratio and Shear Modulus:

Using a lateral extensometer a plot between lateral displacement and external load, was obtained for 0° and 45° specimens. From this plot another plot between lateral strain and external load, as shown in Fig. 3.7, was obtained. Next, a plot between longitudinal strain and load was obtained using a longitudinal extensometer. From these two plots and Eqs. (3.2) and (3.3), the values of ν_{LT} and G_{LT} were computed.

3.6 Results :

The values of various mechanical and photoelastic constants for the new model material were found to be:

V_f = 34.88%

E_L = 25.292 GPa

E_T = 4.6534 GPa

E_{45} = 5.4741 GPa

ν_{LT} = Ø.3877

ν_{TL} = Ø.Ø712

ν_{45} = Ø.3612 GPa

G_{LT} = 2.11Ø3 GPa

F_L = 143.67 N/mm

F_T = 66.591 N/mm

F_{TL} = 54.Ø67 N/mm

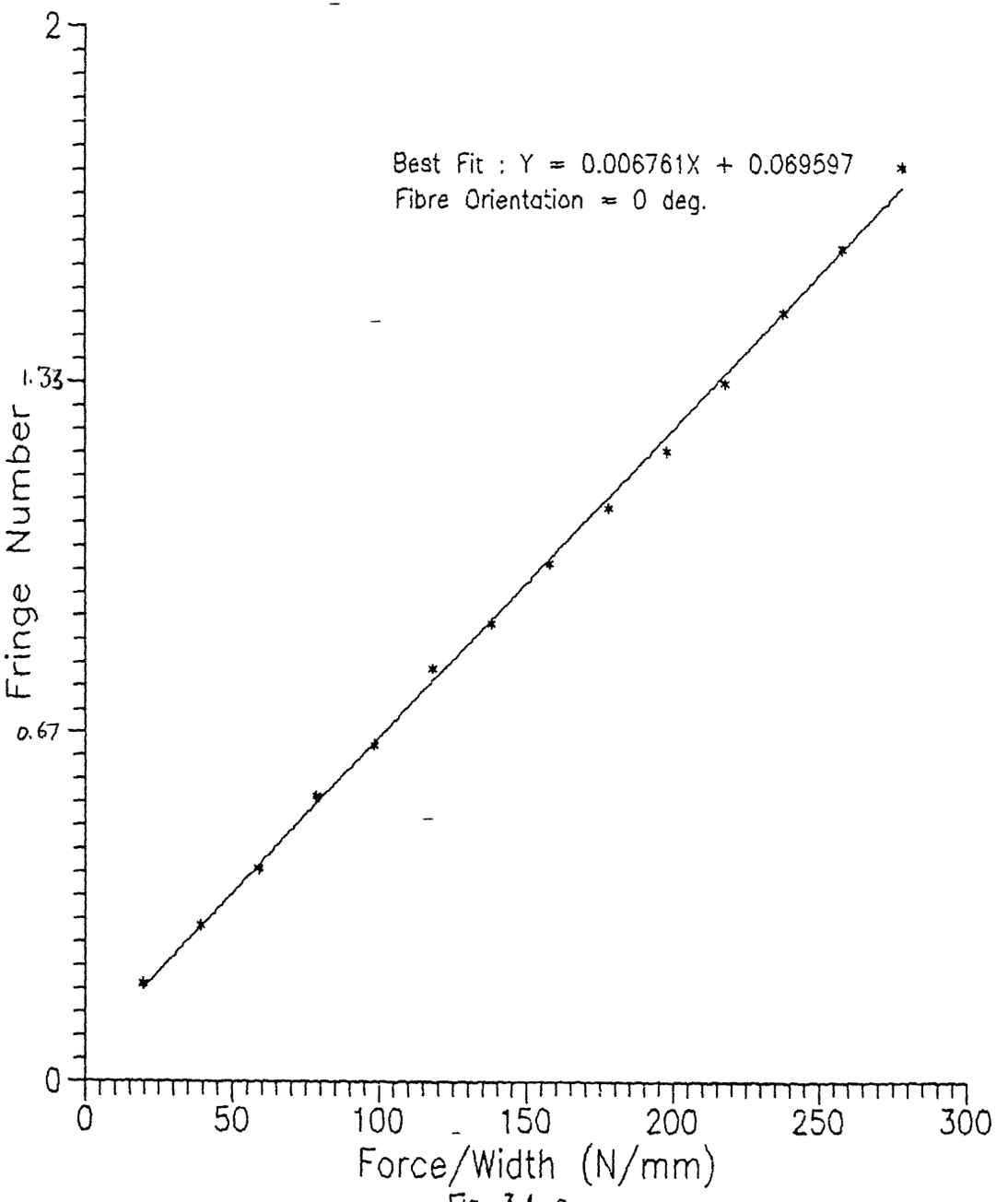
Best Fit : Y = 0.006761X + 0.069597
Fibre Orientation = 0 deg.
Fringe Number
2
1.33
0.67
0
0
50
100
150
200
250
300
Force/Width (N/mm)

Fig. 3.4-a

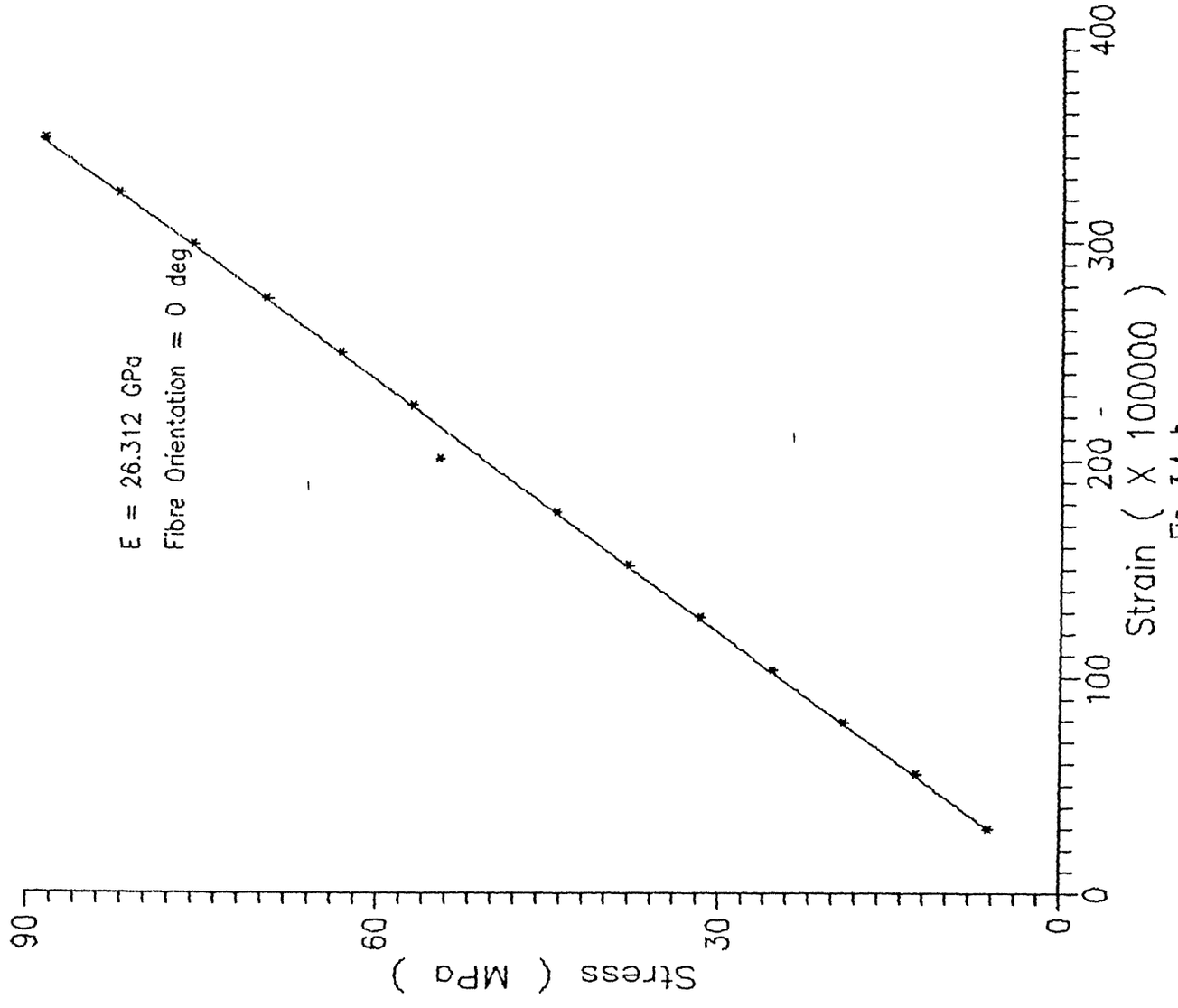
E = 26.312 GPa
Fibre Orientation = 0 deg
Stress (MPa)
Strain (X 100000)
0
30
60
90
0
100
200
300
400

Fig. 3.4-b

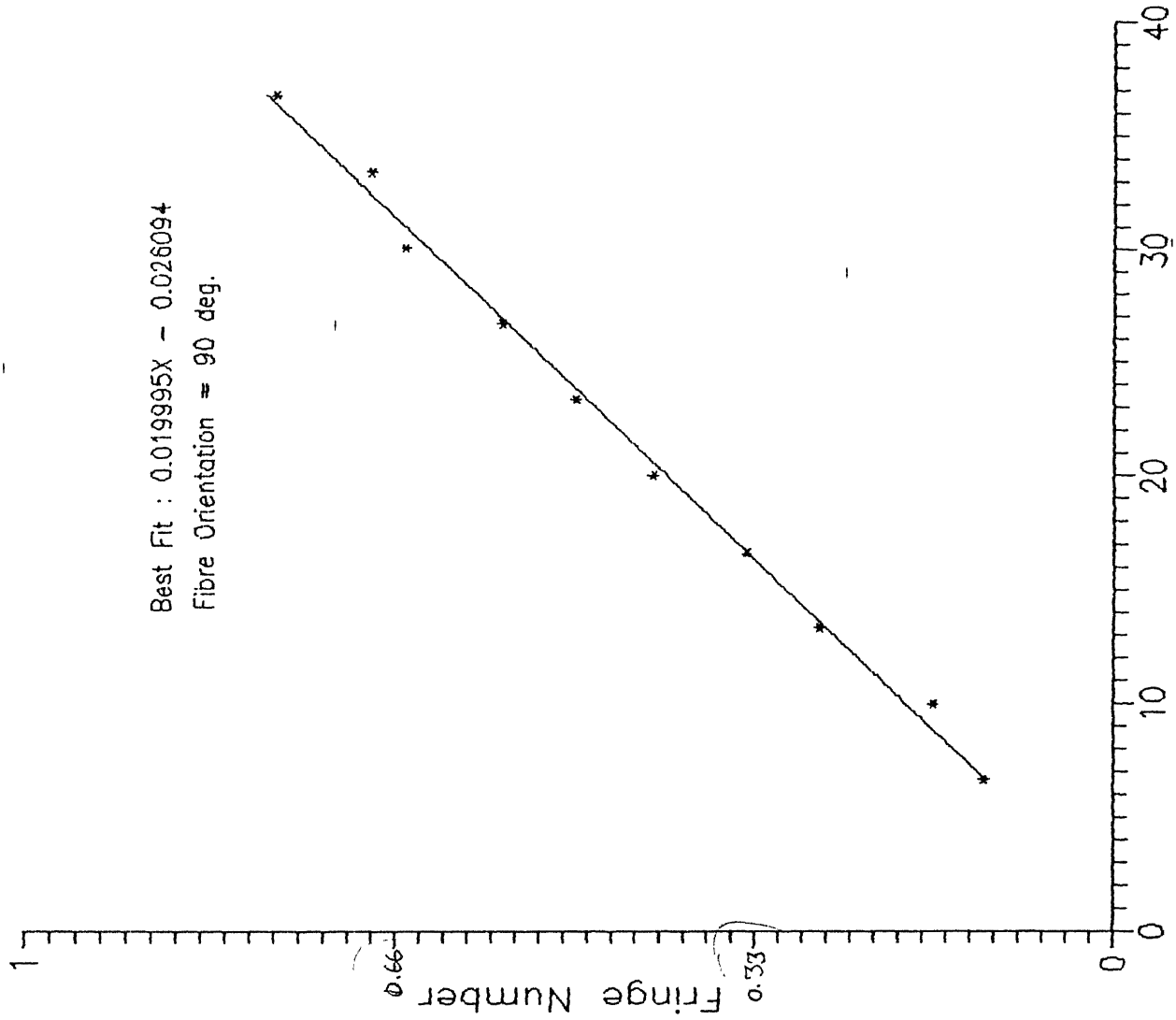
Best Fit : 0.019995X - 0.026094
Fibre Orientation = 90 deg.
Fringe Number
1
0.66
0.33
0
0
10
20
30
40
Force/Width (N/mm)

Fig. 3.5-a

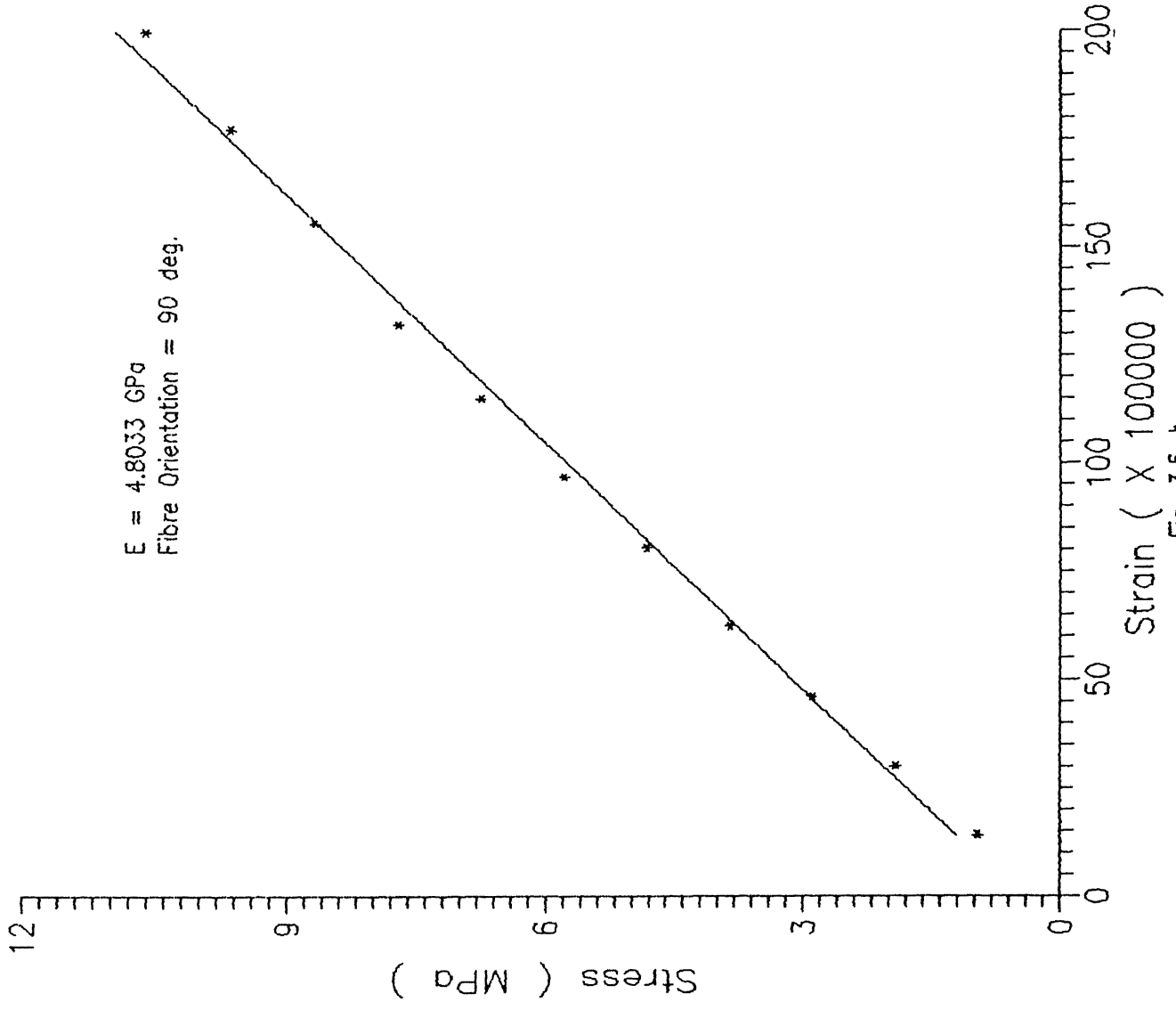
E = 4.8033 GPa
Fibre Orientation = 90 deg.
Stress (MPa)
Strain (X 100000)
0
3
6
9
12
0
50
100
150
200

Fig. 3.5-b

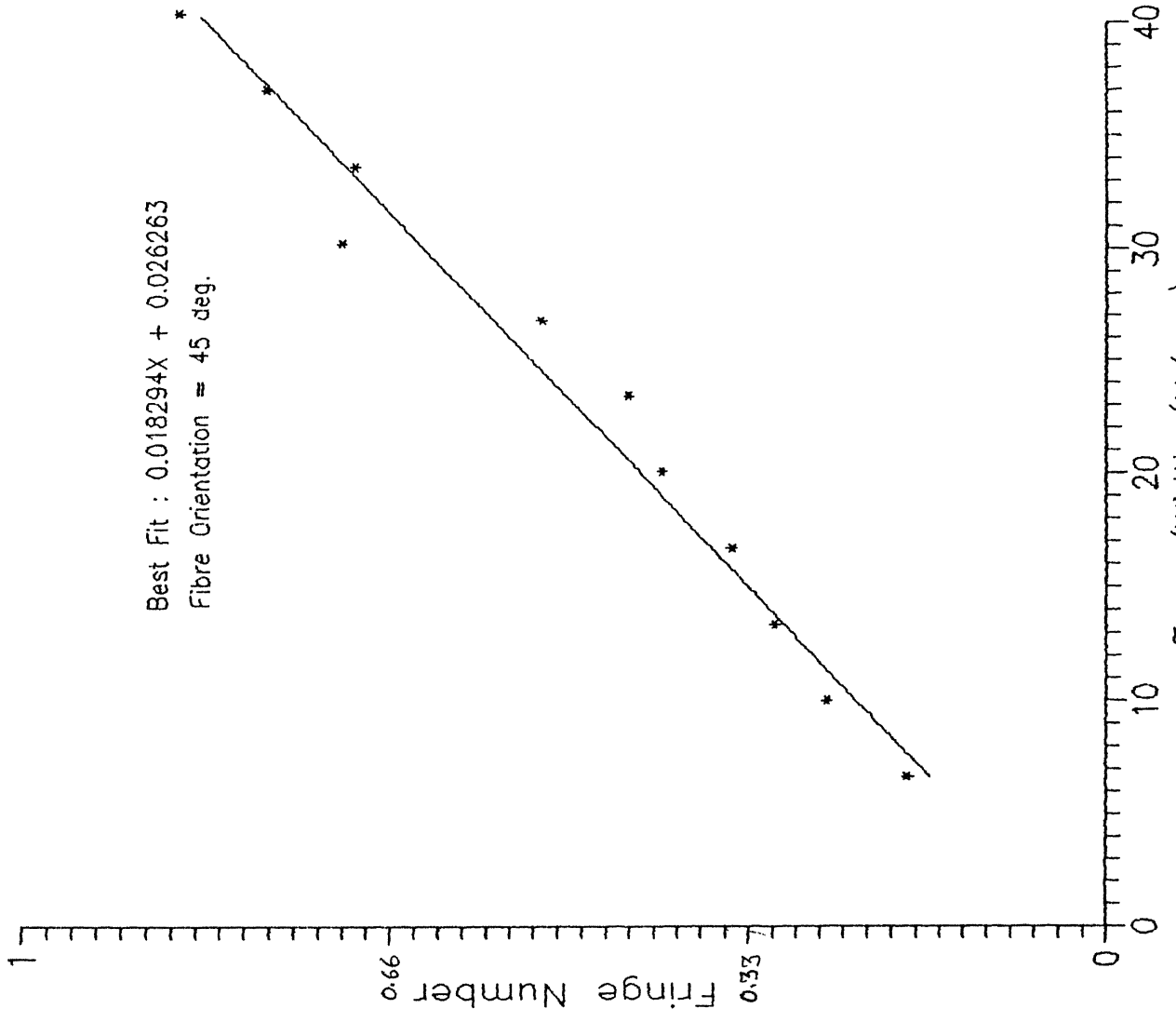
Best Fit : 0.018294X + 0.026263
Fibre Orientation = 45 deg.
Fringe Number
1
0.66
0.33
0
0
10
20
30
40
Force/Width (N/mm)

Fig. 3.6-a

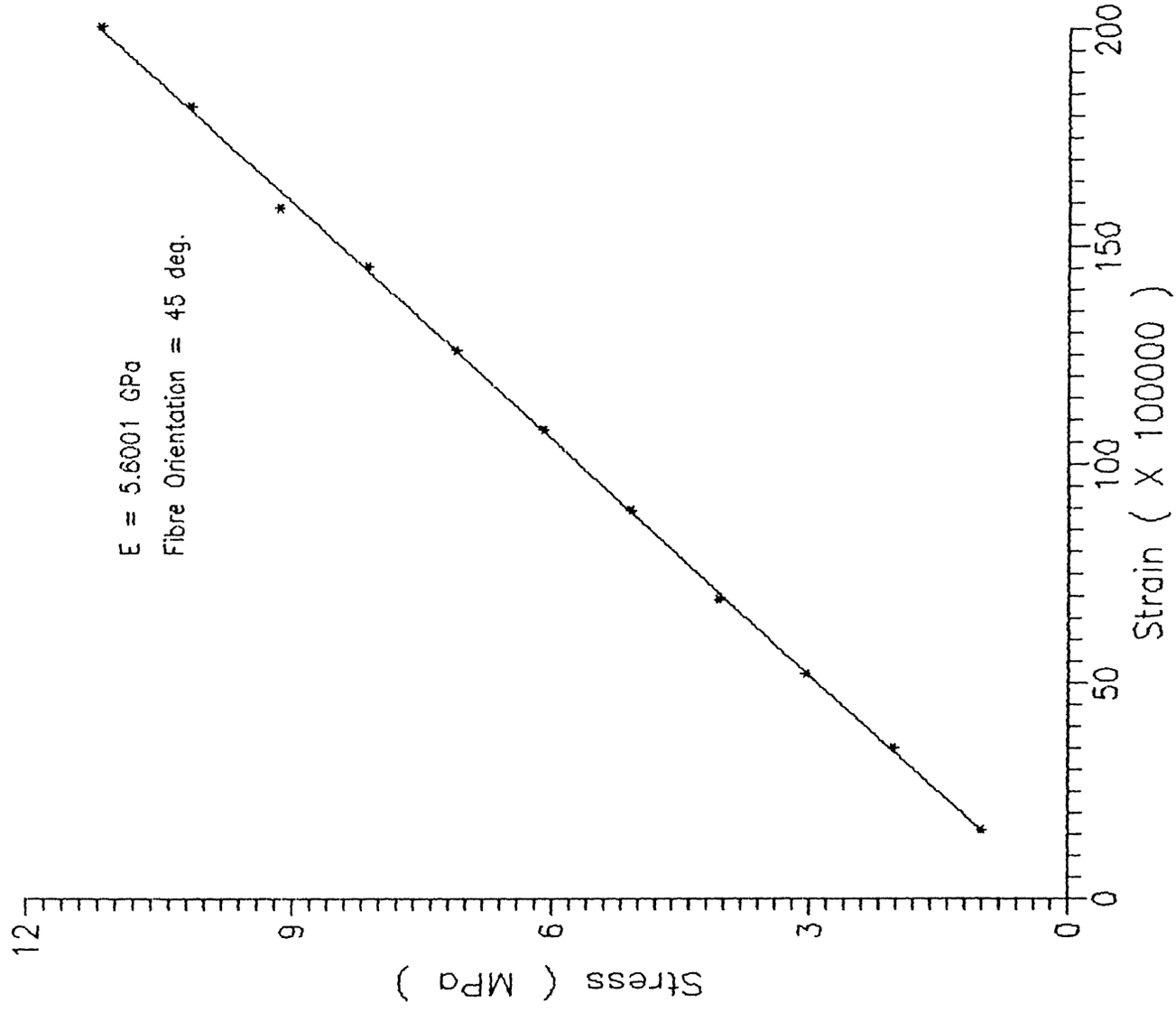
E = 5.6001 GPa
Fibre Orientation = 45 deg.
Stress (MPa)
Strain (X 100000)
0
3
6
9
12
0
50
100
150
200

Fig. 3.6-b

4 EVALUATION OF MODE I STRESS INTENSITY FACTOR:

4.1 Introduction:

The subject of fracture-mechanics is concerned with the study of fracture of materials by crack propagation. The fracture-mechanics approach has been found to be very useful in predicting the strength of isotropic and homogeneous materials in the presence of flaws or cracks and also in developing techniques for quality control and in-service inspection. Fracture mechanics when applied to composite materials is much more complicated because self-similar crack growth, which occurs in homogeneous materials, usually does not occur in composite materials. Another factor which complicates the fracture-mechanics of composites is the presence of local heterogeneity in the material.

It has been has shown that the **strain-energy release rate** for a material during crack growth can be correlated to the the stress distribution in the neighborhood of the crack tip [11]. Further, for isotropic materials, the stress field near a crack tip can be completely defined in terms of a parameter termed, **stress intensity factor**. This parameter is a function of the geometry of the specimen and external loading conditions. Thus, experimental determination of this parameter is very useful in understanding the phenomena of fracture.

Unlike in isotropic materials, for anisotropic materials, the elastic constants vary along with direction. Hence, for composites, the fields for stress, strain and displacement in the vicinity of the crack tip are much more complex.

4.2 Orthotropic Linear Elastic Fracture Mechanics:

The stress analysis ahead of a crack tip in composite materials is a very difficult task as compared to that for isotropic materials. The reasons for this have already been discussed in section 4.1.

In view of these constraints, arriving at a closed form solution for stress field in the vicinity of a crack tip for composites materials is possible only, if it is assumed:

1. The material is homogeneous and orthotropic. This assumption may be justified on the ground that the material may have a flaw (the crack length) whose size is large as compared to that of the local microstructural parameters such as the fiber diameter and the distance between two adjacent fibers.
2. The crack growth is self similar in nature.

With these assumptions, Irwin [18] and Wu [19] have employed Westergaard's differential equation [20] to find the stress field close to the crack tip. The governing equation is:

$$\partial^4 F_1/\partial x_1^4 + \partial^4 F_1/\partial x_1^2 x_2^2 + \partial^4 F_1/\partial x_2^4 = 0$$

Here F_1 is the Airy's stress function.

In this derivation the roots of the auxiliary equation:

$$s^4 - b_2 \cdot s^2 + b_1 = 0 \qquad (4.1)$$

are required. Here:

$$\begin{aligned} b_1 &= a_{11}/a_{22} \\ b_2 &= [2 \cdot a_{12} + a_{66}]/a_{22} \\ a_{11} &= 1/E_{11} \\ a_{12} &= -\nu_{12}/E_{11} = -\nu_{21}/E_{22} \\ a_{22} &= 1/E_{22} \\ a_{66} &= 1/G_{12} \end{aligned} \qquad (4.2)$$

The roots of Eq. (4.1) are either complex or purely imaginary. It was found that for our model material having elastic properties as mentioned in section 3.6, the roots of Eq. (4.1) are purely imaginary. Thus these roots may be expressed as:

$$\left.\begin{array}{ll} s_1 = i\beta_1 & s_2 = -i\beta_1 \\ s_1 = i\beta_2 & s_2 = -i\beta_2 \end{array}\right] \qquad (4.3)$$

With this information Wu [19] derived the crack-tip stress equations as:

$$\sigma_x = \{K_I \cdot \beta_1\beta_2 \cdot [\beta_2 \cdot \cos(Y_2/2)/\sqrt{R_2} - \beta_1 \cdot \cos(Y_1/2)/\sqrt{R_1}]/\sqrt{(2\pi r)} + K_{II} \cdot [\beta_1^2 \cdot \cos(Y_1/2)/\sqrt{R_1} - \beta_2^2 \cdot \sin(Y_2/2)/\sqrt{R_2}]\}/(\beta_1 - \beta_2) + \sigma_{ox} \qquad \textbf{(4.4-a)}$$

$$\sigma_y = \{K_I \cdot [\beta_1 \cdot \cos(Y_1/2)/\sqrt{R_1} - \beta_2 \cdot \cos(Y_2/2)/\sqrt{R_2}]/\sqrt{(2\pi r)} + K_{II} \cdot [\sin(Y_2/2)/\sqrt{R_2} - \sin(Y_1/2)/\sqrt{R_1}]\}/(\beta_1 - \beta_2) \qquad \textbf{(4.4-b)}$$

$$\tau_{xy} = K_{II} \cdot [\beta_2 \cdot \cos(Y_2/2)/\sqrt{R_2} - \beta_1 \cdot \cos(Y_1/2)/\sqrt{R_1}]\}/(\beta_1 - \beta_2) + \{K_I \cdot \beta_1\beta_2 \cdot [\sin(Y_1/2)/\sqrt{R_1} - \sin(Y_2/2)/\sqrt{R_2}]/\sqrt{(2\pi r)} \qquad \textbf{(4.4-c)}$$

where;

$$R_j = \sqrt{[\cos^2\theta + \beta_2 \cdot \sin^2\theta]} \qquad (4.5)$$

$$\text{Tan } Y_j = \beta_j \cdot \text{Tan}\theta \qquad (4.6)$$

with j=1,2.

In Eq. (4.4-a) the σ_{ox} term was added by Mojtahed and Zachary [21]. This additional term takes care of the effect of far field stress applied parallel to the crack. Further, if the crack is parallel to one of the material axes, then the terms involving K_{II} in Eqs. (4.4-a), (4.4-b) and (4.4-c) are irrelevant since in such a case, Mode II is absent.

Eqs. (4.4-a) to (4.4-c) suggest that for the determination of stress intensity factor (S.I.F) one must know the material properties (β_1, β_2) and the state of stress near the crack tip.

The former can be evaluated from the material properties given in section 3.6 of this thesis, while the latter can be evaluated by employing various theoretical or experimental techniques. In the present investigations, the stress field was found out by employing the principles of orthotropic photoelasticity.

4.3 Method for Evaluation of K_I:

4.3.1 Synthesis of Stress Optic Law and Wu's Formulation:

Sampson's stress-optic law is a convenient tool for finding the stress field in the vicinity of a crack tip. The problem of residual stresses, which had not been addressed by Sampson has been taken care of in the following equation:

$$(N/t)^2 = [\sigma_L/F_{\sigma L} - \sigma_T/F_{\sigma T} + N_r \cdot \cos 2\theta_r/t]^2 + [2 \cdot \tau_{LT}/F_{\sigma LT} + N_r \cdot \sin 2\theta_r/t]^2 \quad (4.7)$$

where;

N = fringe order

t = model thickness

N_r = residual fringe order

θ_r = residual isoclinic angle

$F_{\sigma i}$ = stress-optic coefficient

By incorporating Eqs. (4.5) and (4.6) in Eq. (4.7) fringe order (N) can be expressed as:

$$(N/t)^2 = g(K_I, \sigma_{ox}, r, \theta, \beta_1, \beta_2, F_{\sigma i}, N_r, \theta_r) \quad (4.8)$$

For a given model β_1, β_2, $F_{\sigma i}$ are known constants. Thus, Eq. (4.8) can be rewritten as:

$$(N/t)^2 = g(K_I, \sigma_{ox}, r, \theta, N_r, \theta_r) \quad (4.9)$$

Thus the fringe order at any point depends on K_I, σ_{ox}, r, θ, N_r and θ_r. Hence, by finding the fringe order at a large number of points near the crack tip and by employing Eq. (4.9), K_I, σ_{ox}, N_r and θ_r can be found out. The numerical technique used for this purpose is the method of non-linear least squares [22].

4.3.2 Non-Linear Least Squares Method:

Eq. (4.9) can be rewritten as:

$$f(K_I, \sigma_{ox}, r, \theta, N/t, N_r, \theta_r) = \emptyset \qquad (4.10)$$

In this equation r, θ, N/t are known while K_I, σ_{ox}, N_r, θ_r are to be determined. The method of non-linear least squares essentially consists of:

1. Linearizing Eq. (4.10) by a Taylor's series expansion.
2. Applying the criteria of least square to the linearized equations and finally iterating to converge the desired results.

Eq. (4.10) can be rewritten in terms of unknowns as:

$$f_k(K_I, \sigma_{ox}, N_r, \theta_r) = \emptyset \qquad (4.11)$$

where $k = 1,2,\ldots,M$ $(M > 4)$

Taking Taylor's series expansion of (Eq. 4.11) yields:

$$(f_k)_{i+1} = (f_k)_i + (\partial f_k/\partial K_I)_i \cdot \Delta K_I + (\partial f_k/\partial \sigma_{ox})_i \cdot \Delta \sigma_{ox} + (\partial f_k/\partial N_r)_i \cdot \Delta N_r + (\partial f_k/\partial \theta_r)_i \cdot \Delta \theta_k \qquad (4.12)$$

where; i refers to the i^{th} iteration step and K_I, σ_{ox}, N_r, θ_r are corrections to their previous estimates. For the best fit, $(f_k)_{i+1}=\emptyset$. Thus, Eq. (4.12) yields:

$$-(f_k)_i = (\partial f_k/\partial K_I)_i \cdot \Delta K_I + (\partial f_k/\partial \sigma_{ox})_i \cdot \Delta \sigma_{ox} + (\partial f_k/\partial N_r)_i \cdot \Delta N_r + (\partial f_k/\partial \theta_r)_i \cdot \theta_k \qquad (4.13)$$

Eq. (4.13) can be written in matrix form as:

$$\{f\} = [b]\cdot\{\Delta c\} \qquad (4.14)$$

where;

$\{f\}$ = Error vector represented by the RHS of Eq. (4.13)

$[b]$ = Rectangular matrix containing partial derivative terms of Eq. (4.13)

$\{\Delta c\}$ = Correction vector containing K_I, etc.

The correction vector $\{\Delta c\}$ can be evaluated from Eq. (4.14) as:

$$\{\Delta c\} = [d]^{-1}\cdot[b]^{T}\cdot\{f\} \qquad (4.15)$$

where;

$[d] = [b]^{T}\cdot[b]$

The algorithm for evaluating the four unknown parameters in Eq. (4.11) is:

1. Assuming initial values for K_I, σ_{ox}, N_r, θ_r.
2. Computing the elements of matrices {f} and [b] for each of the data point.
3. Computing $\{\Delta c\}$ from Eq. (4.15).
4. Revising the estimates of unknowns i.e.;

$$(K_I)_{i+1} = (K_I)_i + (\Delta K_I)_i \qquad (4.16\text{-a})$$

$$(\sigma_{ox})_{i+1} = (\sigma_{ox})_i + (\Delta\sigma_{ox})_i \qquad (4.16\text{-b})$$

$$(N_r)_{i+1} = (N_r)_i + (\Delta N_r)_i \qquad (4.16\text{-c})$$

$$(\theta_r)_{i+1} = (\theta_r)_i + (\Delta\theta_r)_i \qquad (4.16\text{-d})$$

5. Repeating steps (b), (c), (d) till $\{\Delta c\}$ becomes acceptably small.

4.3.3 Initial Guess for K_I and σ_{ox}:

The algorithm discussed in section 4.4.2 requires a good initial guess for the values of K_I and σ_{ox}. If the initial guess is wide off the mark, then convergence to the exact value is extremely slow. Thus, the following procedure was adopted to get reasonably good estimates of K_I and σ_{ox}.

Putting $\theta=90$ and r=constant; Eqs. (4.4-a) to (4.4-c) give:

$$\sigma_x = A \cdot K_I + \sigma_{ox} \qquad (4.17\text{-a})$$

$$\sigma_y = B \cdot K_I \qquad (4.17\text{-b})$$

$$\tau_{xy} = 0 \qquad (4.17\text{-c})$$

where A and B are constants when r=constant.

Eqs. (4.17-a) to (4.17-c) are simultaneous linear equations. They can be solved for K_I and σ_{ox} with aid of Eq. (4.7) by considering two points in the stress field lying on the contour $\theta=90^{\circ}$.

4.4 Experimental Details:

Two types of specimens were used in this investigation. The geometry of the specimen is shown in Fig. 4.1. One set of model had fibers aligned parallel to the crack-length, while the other set of specimens had fibers running in a direction perpendicular to the crack length. The crack was simulated by using a 0.15 mm milling saw-cutter. Each crack was 6 mm long while the breadth of the specimen was 25 mm. Thus the ratio of crack length (a) specimen width (w) was 0.24. This was necessary since for larger values of a/w ratio, free edge effects modify the stress field significantly.

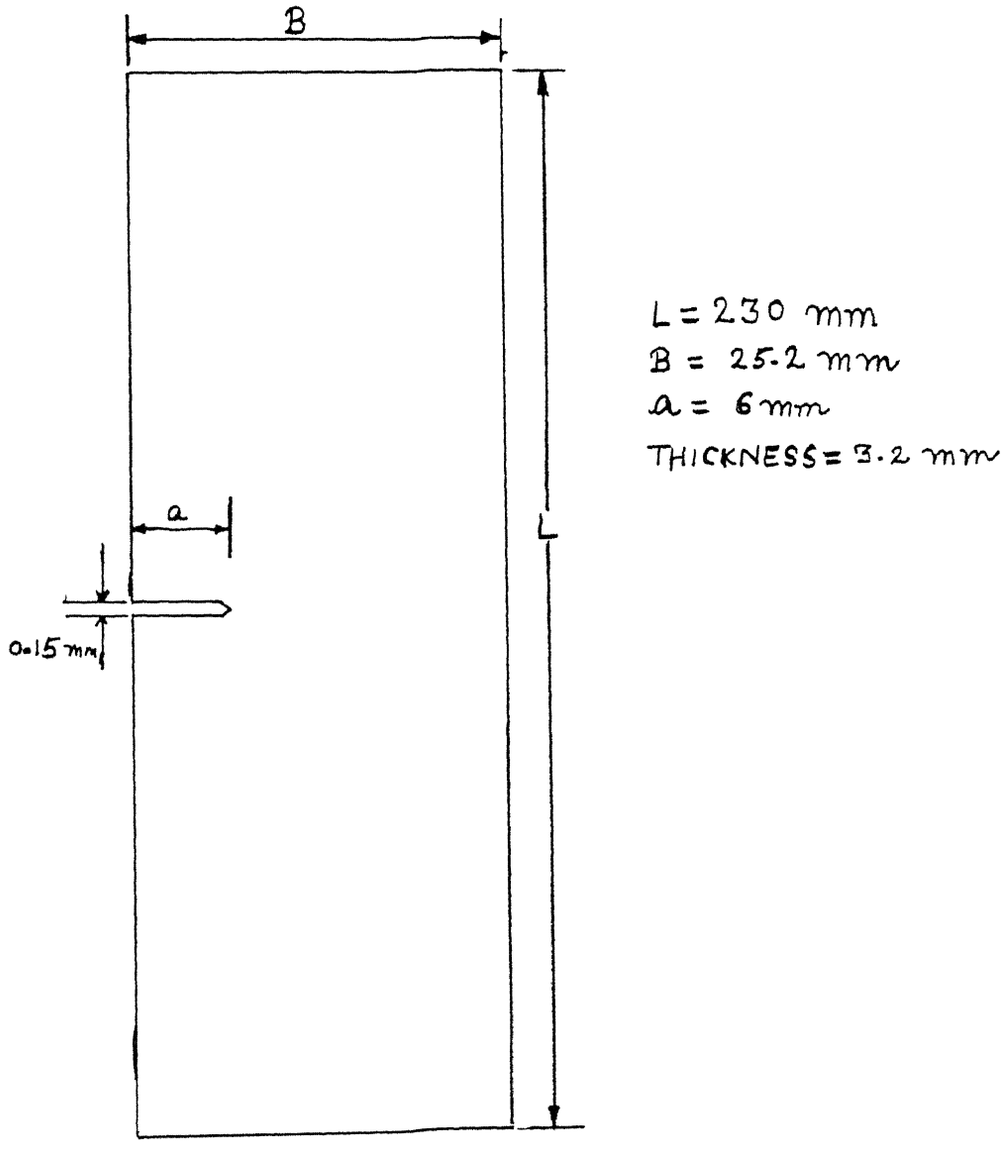

Fig. 4.1 Details of a Single Edge Notched Specimen.

The optical and elastic properties of the model material have been mentioned in section 3.6 of this report. For such a model, the values of nondimensional material properties (β_1, β_2), when crack is perpendicular to the fibers, are:

β_1 = 1.4Ø282

β_2 = Ø.3Ø567

Single edge notched (SEN) specimens were subjected to tensile stresses. This was done using the experimental setup described in section 3.2 of this thesis.

The isochromatic fringe patterns for each specimen were recorded by using a photographic camera. These patterns are shown in Figs. (4.2), (4.3), (4.4). These photographs were later used to collect data points. From each photograph, the details of 3Ø-35 data points were collected. The co-ordinates of each of these points and the corresponding fringe orders were used as the input data field for a program written in FORTRAN used to evaluate the mode I SIF for each of the SEN specimens. The initial value of K_I and σ_{ox} was calculated in the same way as explained in section 4.3.3. The algorithm of the program was same as that given in section 4.3.2. A listing of this program is given in Appendix 1.

4.5 Results:

Following the procedure detailed in section 4.5, the following values of S.I.F in mode I were evaluated:

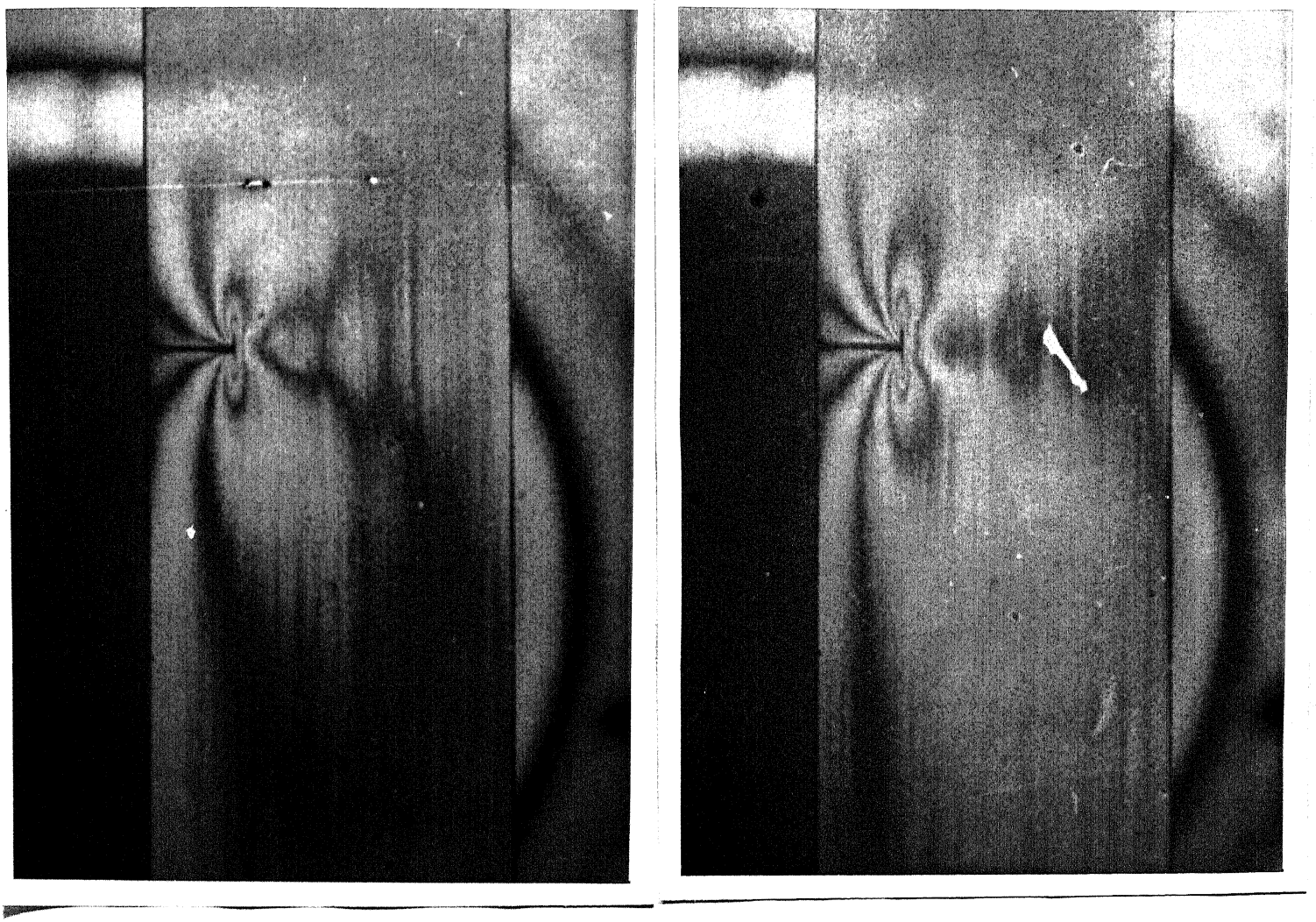

Fig. 4.3: Isochromatics for SEN specimen S_1
(a) σ_L = 37.2 MPa
(b) σ_L = 49.6 MPa

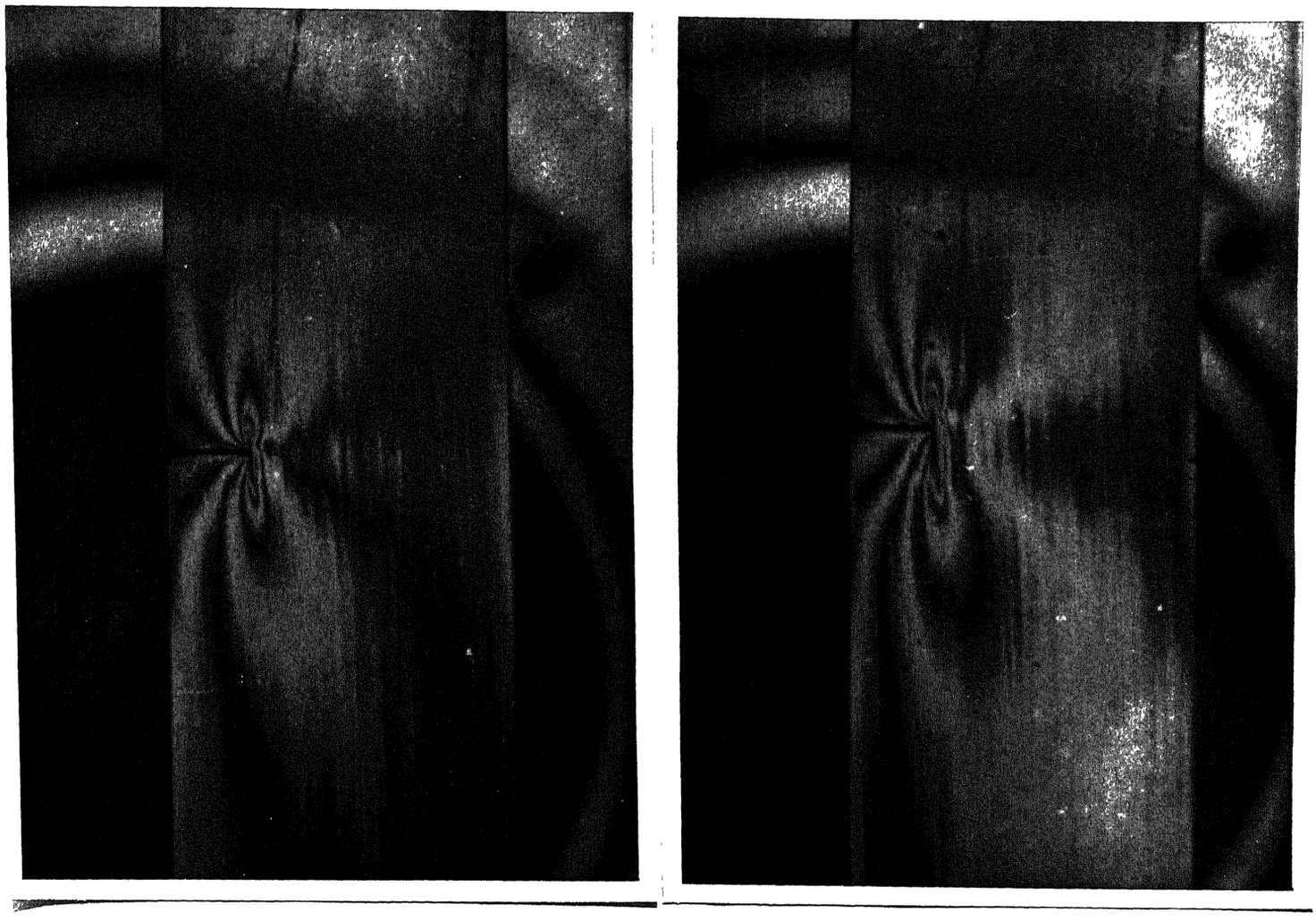

Fig. 4.4: Isochromatics for SEN specimen S_2

(a) σ_L = 37.2 MPa

(b) σ_L = 49.6 MPa

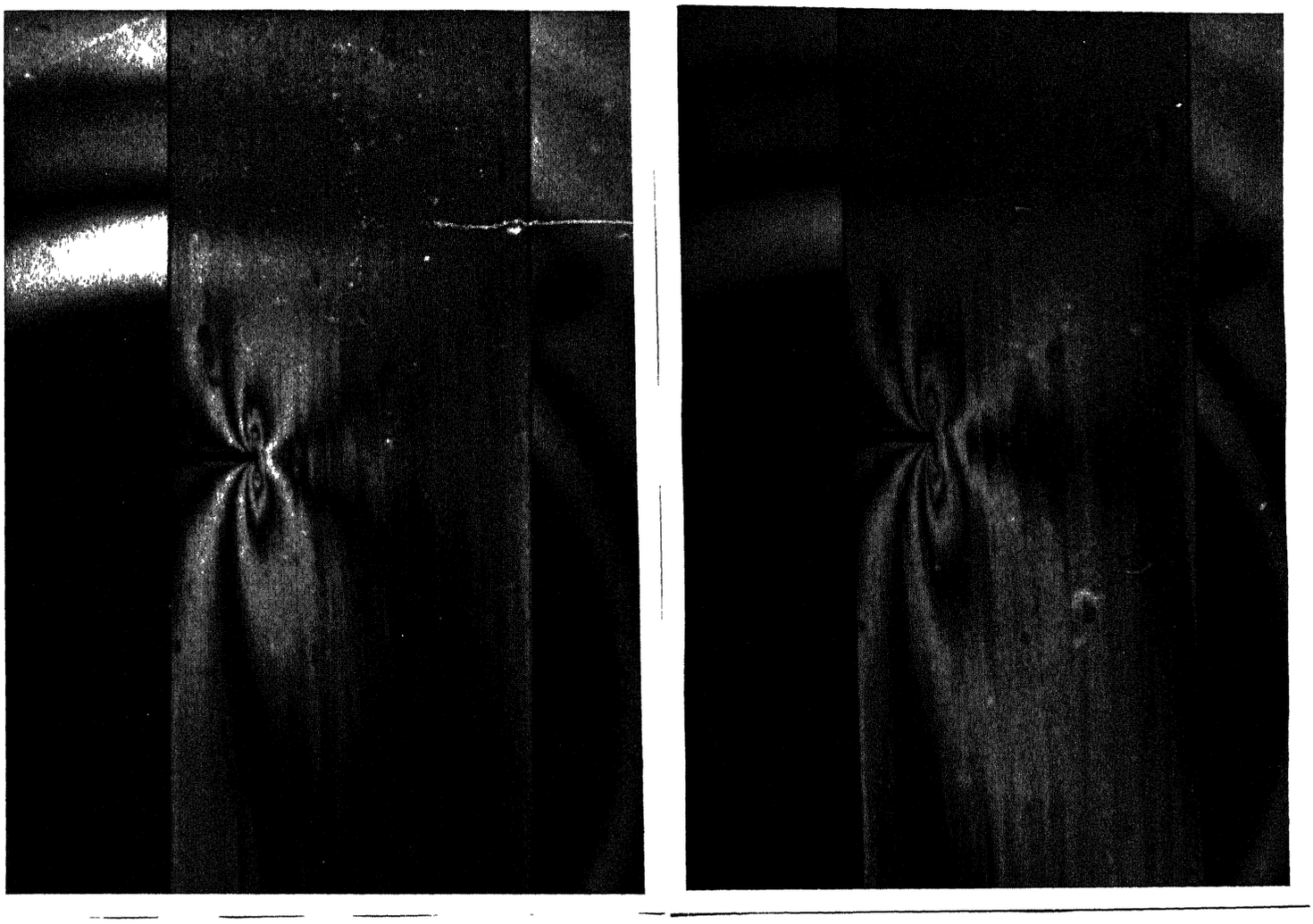

Fig. 4.5: Isochromatics for SEN specimen S_3
(a) σ_L = 37.2 MPa
(b) σ_L = 49.6 MPa

For $\emptyset^{\circ}$ specimens with following material properties:

V_f = 34.88%

E_L = 25.292 GPa

E_T = 4.6534 GPa

E_{45} = 5.4741 GPa

ν_{LT} = Ø.3877

ν_{TL} = Ø.Ø712

ν_{45} = Ø.3612 GPa

G_{LT} = 2.11Ø3 GPa

F_L = 143.67 N/mm

F_T = 66.591 N/mm

F_{TL} = 54.Ø67 N/mm

Initial guess for K_I = 6.2 MPa$\sqrt{m}$

Initial guess for σ_{ox} = 49.4 MPa

the values of S.I.F and σ_{ox} were :

Stress (σ_L) (MPa)	S.I.F (K_I) (MPa$\sqrt{m}$)	Far Field Stress (σ_{ox}) (MPa)
37.2Ø24	6.112	36.91
49.6Ø32	7.91Ø	43.88

For $9\emptyset^{\circ}$ specimens, the value of SIF could not be evaluated. The reason for this was that the low strength of composite in transverse direction. Hence, the specimens fractured at loads which were so low that the maximum fringe order hardly exceeded one.

Using these values of SIF and Eqs. (4.4), the stress field near the crack-tip was determined. The representative plots of σ_L, σ_T and τ_{LT} with respect to the distance from the crack-tip have been shown in Figs. 4.5, 4.6, 4.7.

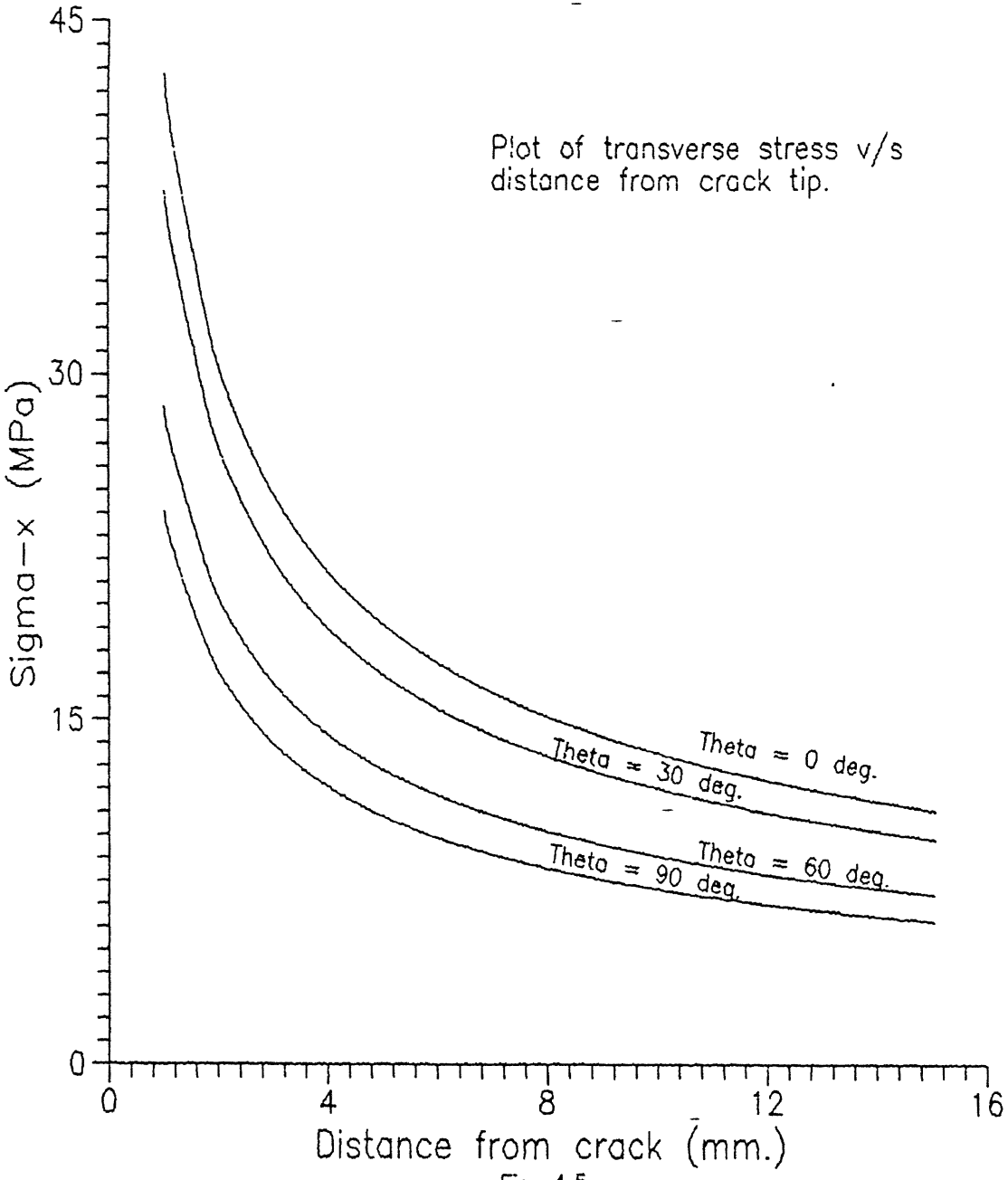
Plot of transverse stress v/s
distance from crack tip.
Sigma-x (MPa)
45
30
15
0
0
4
8
12
16
Distance from crack (mm.)
Theta = 0 deg.
Theta = 30 deg.
Theta = 60 deg.
Theta = 90 deg.

Fig. 4.5

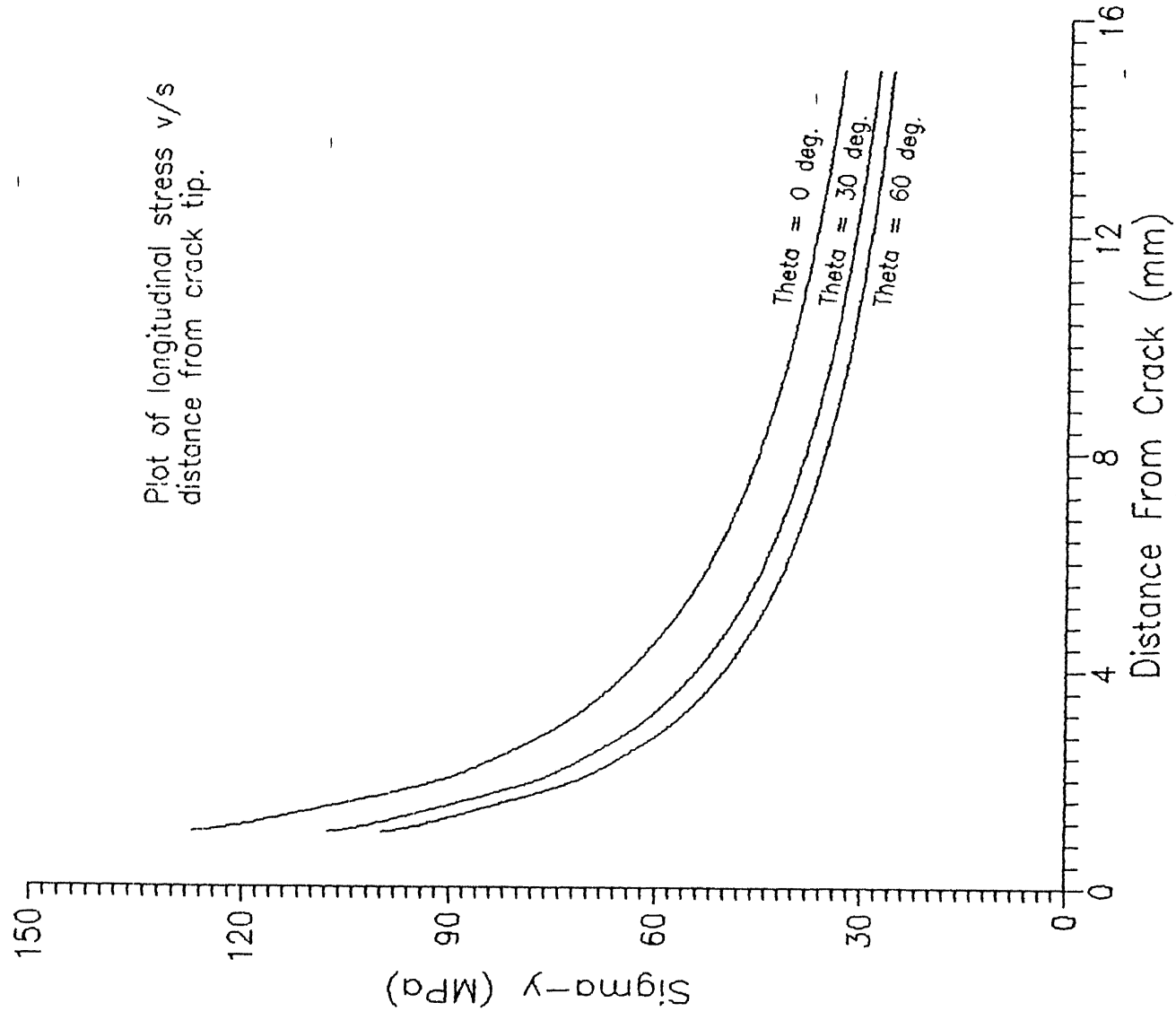
Plot of longitudinal stress v/s distance from crack tip.
Sigma-y (MPa)
150
120
90
60
30
0
0
4
8
12
16
Distance From Crack (mm)
Theta = 0 deg.
Theta = 30 deg.
Theta = 60 deg.

Fig. 4.6

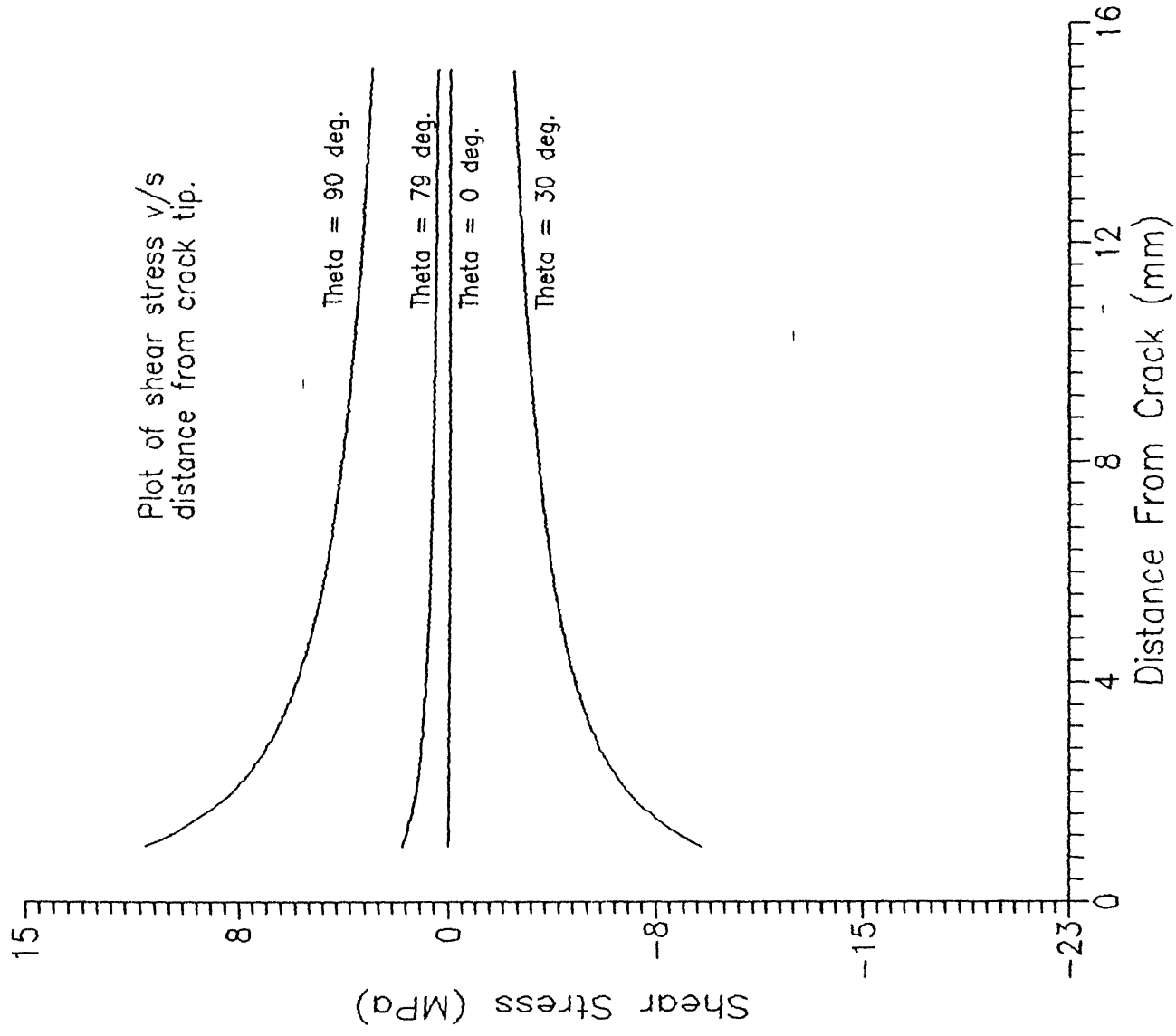
Plot of shear stress v/s
distance from crack tip.
Theta = 90 deg.
Theta = 79 deg.
Theta = 0 deg.
Theta = 30 deg.
Shear Stress (MPa)
15
8
0
-8
-15
-23
0
4
8
12
16
Distance From Crack (mm)

Fig. 4.7

5 CONCLUSIONS:

Increasing importance of fiber composites in various technological applications, calls for an accurate and efficient fracture analysis. For this purpose, the method of transmission photoelasticity can be an extremely powerful and reliable tool. In the present thesis, principles of photo-orthotropic elasticity have been employed successfully to understand the phenomena of fracture in composites. In this context, the following conclusions are in order:

1. A number of formulations for the fabrication of transparent composites as model materials for photoelastic study of composites have been reported in the literature. However, their properties especially transparency were not sufficient for the present investigations. The need of such materials is all the more acute if study of dynamic fracture in composites is intended. In the present investigations, a new model material for photo-orthotropic elastic studies has been developed. The optical properties of this model material as compared to those of other model materials are much better. The properties of the model are:

   Transmission ratio = 69%

   $F_{\sigma L}$ = 143.67 N/mm

   $F_{\sigma T}$ = 66.67 N/mm

   $F_{\sigma LT}$ = 54.Ø7 N/mm

2. The properties mentioned above can be modified by changing the volume fraction of the composite.

3. Using this model material, and by employing principles

of orthotropic photoelasticity and orthotropic linear elastic fracture mechanics, the value of Stress Intensity Factor at different loads has been determined successfully.

4. Comparing these values of S.I.F with the initial guess, it was inferred that the the values of stress intensity factor calculated as explained earlier, were reasonably correct.

5. Using this value of S.I.F and making use of stress-field equations, the variation of σ_x, σ_y and τ_{xy} with respect to the distance from crack tip was plotted.

6. Examination of these plots revealed the presence of a singularity near the crack tip. Further, it was found out, that reversal in the sign of shear stress occurs near the crack tip, when θ increases from 0° to 90°.

REFERENCES

1. **Agarwal, B. D. and Broutman, L. J.,** Analysis and Performance of Fiber Composites, John Wiley (198Ø).
2. **Pih, H. and Knight, C. E.,** "Photoelastic Analysis of Anisotropic Fiber Reinforced Composites", J. Comp. Materials, Vol. 3(1), pp 94-1Ø7, (1969).
3. **Sampson, R. C.,** "A Stress-Optic Law for Photoelastic Analysis of Orthotropic Composites", Exp. Mech., Vol. 1Ø(5), pp 21Ø-215, (197Ø).
4. **Dally, J. W. and Prabhakaran, R.,** "Photo-Orthotropic Elasticity", Exp. Mech., Vol. 11(8), pp 346-356, (1971).
5. **Ranney, M. W.,** Reinforced Composites from Polyesters, Noyes Data Corporation, N. Jersey, U.S.A, (1972).
6. **Pipes, R. B. and Rose, J. L.,** "Strain-Optic Law for a Certain Class of Birefringent Composite", Exp. Mech., Vol. 14(9), pp. 355-36Ø, (1974).
7. **Agarwal, B. D. and Chaturvedi, S. K.,** "Improved Birefringent Composites and Assessment of Photoelastic Theories", Fiber Sci. & Tech., Vol. 11, pp. 399-412, (1978).
8. **Chaturvedi, S. K.,** "Some Experimental Stress Analysis Techniques for Fibrous Composites", Ph. D. Thesis, Dept. of Mech. Engg., IIT, Kanpur, (1978).
9. **Horridge, G. A.,** " A polarized Light Study of Glass Fiber Laminates", Brit. J. Appl. Phys., Vol. 6, pp. 314-319, (1955).
1Ø. **Liebowitz, H.,** Fracture I-VII, Academic Press Inc., N. York, (1968).
11. **Broek, D.,** Elementary Engineering Fracture Mechanics, Martinus Nijhoff Publications, Boston, MA, (1982).
12. **Kobayashi, A. S.,** Experimental Techniques in Fracture Mechanics 1 & 2, The Iowa State Univ. Press, Ames, (1975).
13. **Rolfe, S. T. and Barson, J. M.,** Fracture and Fatigue Control in Structures, Prentice-Hall, Engle Wood Cliffes, N. J., (1977).

14. **Bert, C. W.**, "Theory of Photoelasticity for Birefringent Filamentary Composites", Fiber Sci. and Tech., Vol. 5, pp. 165-71, (1972).

15. **Bhagavantham, S.**, Crystal Symmetry and Physical Properties of Crystals, Academic Press, N. York, (1966).

16. **Agarwal, B. D. and Chaturvedi, S. K.**, "Exact and Approximate Strain-Optic Law for Orthotropic Photoelastic Materials", Fiber Sci. and Tech., Vol. 3(3), pp. 146-150, (1982).

17. **Agarwal, B. D.**, "An Approximate Method of Orthotropic Photoelastic Analysis", Exp. Mech., Vol. 23(1), pp. 55-58, (1983).

18. **Irwin, G. R.**,"Analytical Aspects of Crack Stress Field Problems", TAM Rep. No 213, Univ. of Illinois, (1962).

19. **Wu, E. M.**, "Application of Fracture Mechanics to Orthotropic Plates", TAM Rep. No. 248, Univ. of Illinois, (1963).

20. **Westergaard, H. M.**, J. Appl. Mech., Vol. 6, A49-A53, (1939).

21. **Mojtahed M. and Zachary, L. W.**, "Use of Photoelasticity to Determine Orthotropic K_I Stress-Intensity Factor", Exp. Mech., pp. 184-189, June 1987.

22. **Sanford, R. J.**, "Application of Least-Squares Method to Photoelastic Analysis", Exp. Mech., Vol. 20(6), 192-197, (1980).

APPENDIX-I

Listing of FORTRAN Program for Finding K_I For Composites:

```
C       ***********************************************
C            EVALUATION OF STRESS INTENSITY FACTOR
C       ***********************************************
        IMPLICIT DOUBLE PRECISION (A-H,O-Z)
        DIMENSION DEL(41,4),THT(41),X(41),Y(41),GK(41),RAD(41),PAR(4)
        DIMENSION N(41),SQR(5,5),COL(5,5),TRANS(4,41),GKMIN(41,4),SOL(4)

C       DEFINE THE FUNCTIONS
        PI=3.1429
        FL=143.67E03
        FT=66.59E03
        FLT=54.067E03
        RNR=0.1000
        RTHTT=-0.001

        OPEN (UNIT=51,FILE='FINAL.IN')
        OPEN (UNIT=21,FILE='SIFF.OUT')
        READ(51,*)IA,P,B
        READ(51,*)NPT,T,X0,Y0,REALK1,SIG0X

        STRESS=P/(B*T)/1.0E+06
        WRITE(6,1)IA,STRESS
        WRITE(21,1)IA,STRESS
1       FORMAT('Crack length : ',I2, ' mm.',/,
     $  'Applied stress (e) : ',F7.3)
        M=4
        ITR=0
        PAR(1)=REALK1
        PAR(2)=RNR
        PAR(3)=RTHTT
        PAR(4)=SIG0X
        WRITE(6,2)PAR(1)/1.0E06,PAR(2),RTHTT,(SIG0X/1.0E+06)
        WRITE(21,2)PAR(1)/1.0E06,PAR(2),RTHTT,(SIG0X/1.0E+06)
2       FORMAT('Initial Guess for K_1 = ',F6.4,' MPa√m',/,
     $  'N_r = ',F6.4,/,'θ_r = ',F6.4,/,'σ_ox = ',F7.3,' MPa')

        DO 10 I=1,NPT
        READ(51,*)X(I),Y(I),N(I)
        CALL RADIUS(I,X,Y,X0,Y0,RADD,THTT)
        RAD(I)=RADD
        THT(I)=THTT
10      CONTINUE

11      RNR=PAR(2)
        RTHTT=PAR(3)
        SIG0X=PAR(4)
        DO 20 I=1,NPT
        RADD=RAD(I)
        THTT=THT(I)
```

```
      CALL FUNC(I,N,PAR,THTT,RADD,FL,FT,FLT,T,GK)
      DO 15 J=1,M
      CALL DELT(I,J,N,PAR,X,Y,FL,FT,FLT,T,GK,DELTA)
      DEL(I,J)=DELTA
15    CONTINUE
2Ø    CONTINUE

C     GENERATE THE TRANSPOSE OF DEL MATRIX
      DO 25 I=1,NPT
      DO 3Ø J=1,M
      TRANS(J,I)=DEL(I,J)
3Ø    CONTINUE
25    CONTINUE

C     MULTIPLY TRANS & DEL TO GET 4 X 4 MATRIX
      CALL MATMPY(TRANS,DEL,SQR,M,NPT,M)
C     EVALUATION OF [ TRANSPOSE * COLUMN VECTOR ]
      DO 4Ø I=1,NPT
      GKMIN(I,1)=-GK(I)
4Ø    CONTINUE

      CALL MATMPY(TRANS,GKMIN,COL,M,NPT,1)
C     SOLVING FOR CORRECTIONS IN THE VALUES OF Ki etc.
      DO 43 I=1,M
      SQR(I,M+1)=COL(I,1)
43    CONTINUE

      MP1=M+1
      CALL CHLSKY(SQR,M,MP1,SOL)
      RMAX=ABS(SOL(1)/PAR(1))

      DO 5Ø I=1,M
      PAR(I)=PAR(I)+SOL(I)
      RATIO=ABS(SOL(I)/PAR(I))
      IF (RATIO .GE. RMAX) RMAX=RATIO
5Ø    CONTINUE
      ITR=ITR+1
      WRITE(6,59)ITR
      WRITE(21,59)ITR
      WRITE(6,6Ø)PAR(1)/1.ØEØ6,PAR(2),PAR(3),PAR(4)/1.ØE+Ø6
      WRITE(21,6Ø)PAR(1)/1.ØEØ6,PAR(2),PAR(3),PAR(4)/1.ØE+Ø6
      IF ( RMAX .LE. 1.ØE-Ø4 ) GOTO 55
      GOTO 11
55    WRITE(6,6Ø)PAR(1)/1.ØEØ6,PAR(2),PAR(3),PAR(4)/1.ØE+Ø6
      WRITE(21,6Ø)PAR(1)/1.ØEØ6,PAR(2),PAR(3),PAR(4)/1.ØE+Ø6
59    FORMAT('Iteration no. :',I2,/)
6Ø    FORMAT(/,'K_1 = ',F14.6,' MPa√m',/,'N_r = ',F6.4,
     $ /,'θ_r = ',F6.4,/,'σ_ox = ',F7.3,' MPa')
      STOP
      END
```

```
C       ************************************************
C            SUBROUTINE FOR THE VALUE OF RAD & THETA
C       ************************************************
        SUBROUTINE RADIUS(I,X,Y,XØ,YØ,RADD,THTT)
        IMPLICIT DOUBLE PRECISION (A-H,O-Z)
        DIMENSION X(41),Y(41)
        PI=3.1429
        RADD=SQRT((X(I)-XØ)**2+(Y(I)-YØ)**2)
        IF ( (X(I)-XØ) .EQ. Ø) THTT=Ø.Ø
        IF ( (X(I)-XØ) .EQ. Ø) GOTO 1
        THTT=ABS(ATAN((Y(I)-YØ)/(X(I)-XØ)))
        IF ((X(I) .LT. Ø) .AND. (Y(I) .GE. Ø)) THTT=PI/2.Ø+THTT
        IF ((X(I) .LT. Ø) .AND. (Y(I) .GE. Ø)) GOTO 1
        IF ((X(1) .GT. Ø) .AND. (Y(I) .LT. Ø)) THTT=Ø.Ø-THTT
        IF ((X(I) .GT. Ø) .AND. (Y(I) .LT. Ø)) GOTO 1
        IF ((X(I) .LT. Ø) .AND. (Y(I) .LT. Ø)) THTT=PI+THTT
1       CONTINUE
        RETURN
        END
C       ********************************************
C            SUBROUTINE FOR THE VALUE OF Gk
C       ********************************************
        SUBROUTINE FUNC(I,NN,XX,THTT,R,EL,ET,ELT,FF,G)
        IMPLICIT DOUBLE PRECISION (A-H,O-Z)
        DIMENSION NN(41),G(41),XX(4)
        PI=3.1429
        B2=1.4Ø2818
        B1=Ø.3Ø56674
        F=1.Ø/SQRT(2.Ø*PI*R)
        C=B1*B2*F/(B2-B1)
        D=F/(B2-B1)
        RO1=(COS(THTT)**2+B1*((SIN(THTT))**2))**Ø.25
        RO2=(COS(THTT)**2+B2*((SIN(THTT))**2))**Ø.25
        GA1=ATAN(B1*TAN(THTT))
        GA2=ATAN(B2*TAN(THTT))
        SI1=SIN(GA1/2.Ø)
        SI2=SIN(GA2/2.Ø)
        CO1=COS(GA1/2.Ø)
        CO2=COS(GA2/2.Ø)
        SIGMAX=XX(1)*C*(B2*CO2/(RO2)-B1*CO1/(RO1))+XX(4)
        SIGMAY=XX(1)*D*(B2*CO1/(RO1)-B1*CO2/(RO2))
        TOWXY=XX(1)*C*(SI1/(RO1)-SI2/(RO2))
        AA=XX(2)*COS(2.Ø*XX(3))/FF
        BB=XX(2)*SIN(2.Ø*XX(3))/FF
        A=(SIGMAY/EL-SIGMAX/ET+AA)**2
        B=(2*TOWXY/ELT+BB)**2
        G(I)=SQRT(A+B)-NN(I)/FF
        RETURN
        END
```

```
C       ****************************************************
C            SUBROUTINE FOR THE VALUE OF DIFFERENTIALS
C       ****************************************************
        SUBROUTINE DELT(I,J,NN,PAR,X,Y,FL,FT,FLT,T,GK,DELTA)
        IMPLICIT DOUBLE PRECISION (A-H,O-Z)
        DIMENSION NN(41),PAR(4),X(41),Y(41),GK(41),GKK(41),PR(4)
        MM=4
        DO 1Ø ITR=1,MM
        PR(ITR)=PAR(ITR)
1Ø      CONTINUE
        PR(J)=(1-1.ØE-Ø6)*PR(J)
        XØØ=Ø.454545476135205D-ØØ3
        YØØ=Ø.454545476135205D-ØØ3
        CALL RADIUS(I,X,Y,XØØ,YØØ,RADD,THTT)
        CALL FUNC(I,NN,PR,THTT,RADD,FL,FT,FLT,T,GKK)
        DELTA=(GK(I)-GKK(I))/(1.ØE-Ø6*PAR(J))
        RETURN
        END
C       ****************************************************
C            SUBROUTINE FOR MULTIPLICATION OF MATRICES
C       ****************************************************
        SUBROUTINE MATMPY(A1,B1,C1,M,NNN,L)
        IMPLICIT DOUBLE PRECISION (A-H,O-Z)
        DIMENSION A1(4,41),B1(41,4),C1(5,5)
        DO 2 I=1,M
        DO 2 J=1,L
        C1(I,J)=Ø.Ø
        DO 1 K=1,NNN
        C1(I,J)=C1(I,J)+A1(I,K)*B1(K,J)
1       CONTINUE
2       CONTINUE
        RETURN
        END
C       ****************************
C            SUBROUTINE CHLSKY
C       ****************************
        SUBROUTINE CHLSKY(A,N,M,X)
        IMPLICIT DOUBLE PRECISION (A-H,O-Z)
        DIMENSION A(5,5),X(4)

C       CALCULATE THE FIRST ROW OF UPPER UNIT TRI. MATRIX

        DO 3 J=2,M
3       A(1,J)=A(1,J)/A(1,1)

C       EVALUATION OF OTHER ELEMENTS OF U & L MATRICES

        DO 8 I=2,N
        J=1
        DO 5 II=J,N
        SUM=Ø.ØDØØ
        JM1=J-1
        DO 4 K=1,JM1
4       SUM=SUM+A(II,K)*A(K,J)
5       A(II,J)=A(II,J)-SUM
```

```
        IP1=I+1
        DO 7 JJ=IP1,M
        SUM=Ø.ØDØØ
        IM1=I-1
        DO 6 K=1,IM1
6       SUM=SUM+A(I,K)*A(K,JJ)
7       A(I,JJ)=(A(I,JJ)-SUM)/A(I,I)
8       CONTINUE

C       SOLVE FOR X(I) BY BACK SUBSTUTION
        X(N)=A(N,N+1)
        L=N-1
        DO 1Ø NN=1,L
        SUM=Ø.Ø
        I=N-NN
        IP1=I+1
        DO 9 J=IP1,N
9       SUM=SUM+A(I,J)*X(J)
1Ø      X(I)=A(I,M)-SUM
        RETURN
        END
```